NASA TECHNICAL NOTE

NASA TN D-8521

NASA TN D-8521

A COMPARISON OF THE RESULTS OF DYNAMIC WIND-TUNNEL TESTS WITH THEORETICAL PREDICTIONS FOR AN AEROMECHANICAL GUST-ALLEVIATION SYSTEM FOR LIGHT AIRPLANES

Eric C. Stewart and L. Tracy Redd

Langley Research Center
Hampton, Va. 23665

NATIONAL AERONAUTICS AND SPACE ADMINISTRATION · WASHINGTON, D. C. · SEPTEMBER 1977

NASA TN D-8521

1. Report No.	2. Government Accession No.	3. Recipient's Catalog No.
NASA TN D-8521		

4. Title and Subtitle	5. Report Date
A COMPARISON OF THE RESULTS OF DYNAMIC WIND-TUNNEL TESTS WITH THEORETICAL PREDICTIONS FOR AN AEROMECHANICAL GUST-ALLEVIATION SYSTEM FOR LIGHT AIRPLANES	September 1977
	6. Performing Organization Code
7. Author(s)	8. Performing Organization Report No.
Eric C. Stewart and L. Tracy Redd	L-11352
	10. Work Unit No.
9. Performing Organization Name and Address	505-10-11-02
NASA Langley Research Center Hampton, VA 23665	11. Contract or Grant No.
	13. Type of Report and Period Covered
12. Sponsoring Agency Name and Address	Technical Note
National Aeronautics and Space Administration Washington, DC 20546	14. Sponsoring Agency Code

15. Supplementary Notes

16. Abstract

Dynamic wind-tunnel tests have been conducted on a 1/6-scale model of a general-aviation airplane equipped with an all-mechanical gust-alleviation system which uses auxiliary aerodynamic surfaces to drive the flaps. The longitudinal short-period motions were studied under simulated gust conditions in order to (1) verify the mathematical model used in a previous study to predict the performance of the full-scale system and (2) determine the amount of normal-acceleration alleviation which could be attained. The model responses were measured for different configurations with the system active and without the system active for comparison. The tests confirmed the general relationships between the experimental variables and the model responses predicted by the mathematical model, but there were significant differences in the magnitudes of the responses.

The experimental results for the model were used to estimate a reduction of 30 percent in the rms normal-acceleration response of a similar full-scale airplane in atmospheric turbulence.

17. Key Words (Suggested by Author(s))	18. Distribution Statement
Dynamic wind-tunnel tests Gust alleviation Gust response Light airplane Turbulence	Unclassified - Unlimited Subject Category 01

19. Security Classif. (of this report)	20. Security Classif. (of this page)	21. No. of Pages	22. Price*
Unclassified	Unclassified	45	$4.00

* For sale by the National Technical Information Service, Springfield, Virginia 22161

A COMPARISON OF THE RESULTS OF DYNAMIC WIND-TUNNEL TESTS WITH THEORETICAL PREDICTIONS FOR AN AEROMECHANICAL GUST-ALLEVIATION SYSTEM FOR LIGHT AIRPLANES

Eric C. Stewart and L. Tracy Redd
Langley Research Center

SUMMARY

Dynamic wind-tunnel tests have been conducted on a 1/6-scale model of a general-aviation airplane equipped with an all-mechanical gust-alleviation system which uses auxiliary aerodynamic surfaces to drive the flaps. The longitudinal short-period motions were studied under simulated gust conditions in order to (1) verify the mathematical model used in a previous study to predict the performance of the full-scale system and (2) determine the amount of normal-acceleration alleviation which could be attained. The normal-acceleration response, pitching response, and flap response were measured for different configurations with the system active and without the system active for comparison. The tests confirmed the general relationships between the experimental variables and the model responses predicted by the mathematical model, but there were significant differences in the absolute values of the responses. For example, the pitching response increased when the normal-acceleration response was alleviated as predicted by theory, but the levels of the responses were not accurately predicted by theory. The experimental results for the model were used to estimate a reduction of 30 percent in the rms normal-acceleration response of a similar full-scale airplane in atmospheric turbulence.

INTRODUCTION

The ride of light airplanes in turbulent weather is characteristically rough and uncomfortable. The up-and-down heave motions are especially large because of the low wing loadings of light airplanes. These motions could be alleviated by an automatic system using sensors, computers, and powered servos to drive the airplane's lift-controlling devices. Such a system, however, would probably be too costly and complex for widespread use in the general-aviation fleet at this time. A simpler and potentially less costly alleviation system was built and tested with encouraging results in France some years ago (ref. 1). This all-mechanical system used the horizontal tail surfaces (which were designed to rotate about chordwise axes near the fuselage) to drive the trailing-edge flaps through an internal linkage system. Such mechanical systems appear to offer an inexpensive gust-alleviation capability for light airplanes.

A system somewhat similar to the French design has been proposed recently. It is designed primarily to reduce the heave response to vertical gusts at cruise flight conditions. The present system is also all mechanical, but it uses two auxiliary aerodynamic surfaces rather than the horizontal tail surfaces to drive

the flaps. These auxiliary aerodynamic surfaces are mounted on either side of the fuselage near the leading edge of the wing and are connected by rigid external linkages to the flaps. This design does not require modification to the basic horizontal tail surfaces and should result in shorter, lighter linkages and other advantages compared to the French design.

The presently proposed system has been studied using a radio-controlled model (ref. 2). A subjective evaluation of this model's performance indicated that the system reduced the lift response to angle-of-attack changes; however, no quantitative turbulence response measurements were made. The system has also been studied theoretically (refs. 3, 4, and 5). These theoretical studies predicted that the system would reduce the normal-acceleration response about 50 percent while increasing the pitching response about 100 percent. These predictions, however, were based on an assumed set of ideal flap-response characteristics which might be difficult to achieve in a practical installation. Quantitative experimental data on the performance of the system in gusts were, therefore, needed for two purposes: first, to verify the mathematical model used in the theoretical studies and, second, to see how much alleviation could be attained with a practical system. Dynamic model tests in a simulated gust field were used to provide the required data. The model was dynamically scaled to be representative of a typical light airplane, and the gust-alleviation system was constructed in accordance with typical general-aviation construction practices.

Results of dynamic-model tests conducted in the Langley transonic dynamics tunnel (TDT) are presented. A 1/6-scale model of a single-engine, four-place, light aircraft equipped with the proposed gust-alleviation system was used in the tests. Test variables included the mechanical gearing ratio between the flap and vane, the use or absence of a loading spring, and two different flap-chord lengths. Four different types of tests were conducted: (1) the quasi-static flap response to angle-of-attack changes, (2) the dynamic flap response to disturbances from a trimmed equilibrium position, (3) the dynamic short-period response of the airplane to disturbances from a trimmed condition, and (4) the dynamic-model response to sinusoidal gust disturbances in the frequency range from 0.5 Hz to 4.0 or 5.0 Hz. Three different types of response measurements were made: (1) the normal-acceleration response at the model center of gravity, (2) the pitching response, and (3) the flap-vane response. These measurements were compared to theoretically calculated responses using the mathematical model of reference 5.

SYMBOLS

a constant in Von Karman gust spectrum (1.339)

C_h hinge-moment coefficient, $\dfrac{H}{\frac{1}{2}\rho V^2 S_f c_f}$

C_m pitching-moment coefficient, $\frac{M}{\frac{1}{2}\rho V^2 Sc}$

C_Z vertical-force coefficient, $\frac{Z}{\frac{1}{2}\rho V^2 S}$

c mean aerodynamic chord, m

c_f flap chord, m

f frequency, Hz

g acceleration of gravity, 9.81 m/sec^2

H hinge moment referred to flap hinge line for variables subscripted f and referred to vane hinge line for variables subscripted v, N-m

I_f flap inertia about flap axis (total for both sides), kg-m^2

I_v vane inertia about vane dihedral hinge line (total for both sides), kg-m^2

I_y pitch inertia, kg-m^2

i incidence of vane relative to local flow angle due to trim control, rad (see eq. (A3))

i_r ratio of flap inertia to flap inertia plus vane inertia reflected back to flap axis, $\frac{I_f}{I_f + \gamma^2 I_v}$

K negative of ratio of flap-deflection change to angle-of-attack change, $-\Delta\delta_f/\Delta\alpha$

K_o loading spring torque at zero flap deflection, N-m

K_s loading spring gradient, N-m/rad

K_v static vertical alleviation factor (see eq. (A6))

K_y ratio of pitch radius of gyration to mean aerodynamic chord, k_y/c

k_y pitch radius of gyration, m

L scale length of turbulence assumed to be 1000 m

ℓ ratio of tail length to mean aerodynamic chord

l_n	effective vane length (see eq. (A10)), m
l_v	longitudinal distance from airplane center of gravity to vane quarter chord (vane length), m
M	pitching moment, N-m
m	mass, kg
n	normal acceleration, positive downward, g units
q	pitching velocity, rad/sec; also, dynamic pressure, N/m^2
S	area of wing, m^2
S_f	area of flap, m^2
s	Laplace variable, sec^{-1}
t	time, sec
V	true velocity with respect to undisturbed air mass, m/sec
w_g	vertical velocity of gust, positive upward, m/sec
w_o	increment in vertical velocity with respect to undisturbed air mass, m/sec
Z	vertical force, positive downward, N
α	angle of attack, rad or deg
α_o	increment in angle of attack with respect to undisturbed air mass, w_o/V, rad
γ	flap-vane gearing ratio, $\Delta\delta_v/\Delta\delta_f$
δ_f	flap deflection, positive when trailing edge is down, rad or deg
δ_{gv}	tunnel gust-generating-vane position, deg
δ_v	vane dihedral deflection angle, positive when outboard end is down, rad
ϵ	downwash angle, positive downward, rad
ζ	damping ratio
θ	pitch angle, rad or deg
λ	geometric scale factor of model (equal to 1/6)

μ relative density factor, $m/\rho Sc$

ρ density of air, kg/m^3

σ_n rms normal acceleration, g units

σ_{wg} rms vertical gust velocity, m/sec

Φ_n normal-acceleration power spectral density, $g^2/rad/m$

Φ_{wg} Von Karman gust spectrum for vertical gust velocity, $m^2/sec^2/rad/m$

Ω wave number, ω/V, rad/m

ω frequency, rad/sec

ω_n natural frequency, rad/sec

Subscripts:

f flap

g gust

n normal acceleration

t tail

v vane

w wing

A bar over a symbol denotes the Laplace transform of a variable. Dots over a symbol represent derivatives with respect to time, except in the case of damping derivatives such as $C_{h_{\dot{\delta}_f}}$ where the derivative is defined by the relation

$$C_{h_{\dot{\delta}_f}} = \frac{\delta C_h}{\partial\left(\frac{\dot{\delta}_f c}{2V}\right)}$$

Stability derivatives are indicated by subscript notation; for example,

$$C_{Z_\alpha} = \frac{\partial C_Z}{\partial \alpha}$$

DESCRIPTION OF THE GUST-ALLEVIATION SYSTEM

A sketch of the basic components of the gust-alleviation system is presented in figure 1. Two auxiliary aerodynamic surfaces, or vanes, are mounted on either side of the fuselage near the wing. These vanes are hinged about chordwise axes on either side of the fuselage, permitting the dihedral angle to vary in response to gusts, as shown in the front view of figure 1. The vanes also pivot about a spanwise axis (side view of fig. 1) to change their angle of incidence as a function of stick position in order to provide pilot control. As the vanes move upward (increase their dihedral) in response to an up gust, the flaps are deflected upward by the flap-vane linkages. The flaps decrease the lift on the wing by an amount almost equal to the increase in lift on the wing due to the gust which caused the vane dihedral deflection. In this way the lift on the airplane is maintained relatively constant regardless of the gusts encountered by the airplane. The flaps are interconnected so that they deflect together symmetrically to prevent the system from producing rolling moments.

This gust-alleviation system achieves its alleviation by reducing the lift-curve slope of the airplane to a small value so that there are small changes in lift due to gust-induced angles of attack. This small response to changes in angle of attack would practically eliminate the pilot's ability to change the flight path by using the elevator unless some sort of compensation was provided. The spanwise pivot axis for changing vane incidence and the pilot's control linkage shown in the side view of figure 1 are provided for this purpose. As the elevator is deflected, the vanes are rotated about their quarter-chord lines by an angle equal to, but in the opposite direction from, the change in angle of attack commanded by the elevator deflection. The steady-state angle of attack of the vanes is, therefore, constant; and, except for transients, the flaps do not respond to changes in angle of attack due to elevator-control inputs. However, the flaps still respond to changes in angle of attack due to gusts. Because the primary purpose of this investigation was to study gust response, the flap-elevator interconnection was not implemented on the scale model.

A loading spring is provided so that the vanes do not have to operate at a near zero angle of attack in order to maintain the flap equilibrium position at zero deflection. At a zero vane angle of attack the vane will be generating drag but no lift and will therefore unnecessarily penalize the airplane's performance. The lift on the vane at a positive vane angle of attack must be balanced by the loading spring in order to keep the flap deflection at the center zero position for the trimmed flight condition in the absence of gusts. If the flight condition changes, either the spring preload or the vane incidence relative to the airplane must be readjusted to reposition the flap to zero deflection for the new angle of attack of the airplane. A positive vane angle of attack results in the system alleviating horizontal gusts as well as vertical gusts since the lift on the vanes will change with airspeed. Horizontal gusts are of much less importance than vertical gusts, however, except for low-speed approaches.

TEST EQUIPMENT

Wind Tunnel

The wind-tunnel tests were conducted in the Langley transonic dynamics tunnel (TDT). The tunnel is of the single-return type and is powered by a motor-driven fan. The tunnel has a 4.88-m^2 test section (fig. 2).

Gust-generation system.- The tunnel is equipped with a gust-generating system which has two vanes on each side of the converging section of the tunnel (fig. 3). The vanes have a span of 1.1 m, a taper ratio of 0.5, and an aspect ratio of 1.2. They are sinusoidally oscillated about their quarter chord by a flywheel crank system driven by synchronized hydraulic motors. The vanes can be driven at amplitudes up to $\pm 12^{\circ}$, at frequencies from 0 to 20 Hz. The vortices trailing off the tips of the vanes produce oscillations in the vertical velocity or angle of attack in the test section. See reference 6 for more details on the gust-generating system.

Gust-angle calibration.- A crossed hot-wire anemometer was used to measure the variations of angle of attack produced by the gust-generating vanes. This anemometer was mounted on a remotely controlled sting to facilitate making gust measurements at different locations in the test section. The gust measurements were obtained at the required test conditions with the model and its mounting system removed in order to avoid interference of the model on the measurements. The output of the anemometer was recorded on a frequency modulated (FM) tape recorder. After the tests the recordings were reduced using a real-time analyzer. The real-time analyzer was used in a peak-hold mode which stores the spectrum of the input in 250 filter locations or frequency windows. Subsequent spectrums are taken periodically, but the level in each filter location is updated only in a positive direction; that is, the value in each filter is changed only if the new spectrum value exceeds the present value. In the present application, a 0- to 25-Hz range was used with a resulting frequency resolution of 0.15 Hz.

The measured gust-angle variations on the tunnel centerline at the test station and at two other points, one above and one below the centerline, are shown in figure 4. As can be seen by the data in figure 4, the gust-angle variations at low frequencies for the off-centerline positions were slightly less than at the centerline. Since the center of gravity of the model was not restricted to the centerline of the tunnel or even to the vertical line between the upper and lower probe measurement stations, the true gusts encountered by the model were not exactly known. The spanwise variation of the gusts was not measured because previous tests (ref. 7) showed that, over ± 1 m from the centerline, the variation in the gust angle was about ± 10 percent.

In order to facilitate the subsequent frequency-response calculations for the model, an analytical expression for the gust angle as a function of frequency was derived using the data from all three probe locations. The analytical expression was in the form of a power series with terms up to the fifth power of the frequency, and the coefficients for the terms were determined using a least-squares linear-regression analysis. The data from the centerline were weighted twice as heavily as the off-centerline data because the model was near

the centerline most of the time. The gust angle calculated from this expression is shown by the dashed lines in figure 4.

Dynamic Model

Model description.- The model was a 1/6-scale model of a single-engine, four-place, high-wing light airplane. The dimensions of the model and gust-alleviation system are shown in figure 5. Note in figure 5(b) that the vanes and flaps were mass balanced so that vertical translational accelerations of the model did not cause flap-vane accelerations. The dihedral pivot axes of the vanes and the flap rotation axes were provided with ball bearings to minimize friction. The flaps and vanes had approximately $\pm 20^{\circ}$ travel while the vane incidence had $\pm 15^{\circ}$ travel. An adjustable bellcrank system, which was mounted under the wing as shown in figure 6, made it possible to vary the gearing ratio between the vane and flap.

Scaling.- Table I lists the pertinent physical characteristics of the model, the test velocity, and the dynamic-response scaling factors. The scale factors for all the parameters in table I were based on maintaining constant Froude number V^2/gc and relative density factor $m/\rho Sc$ between model and full-scale airplane. Inasmuch as the model was flown at atmospheric density and in the same gravitational field as the full-scale airplane, the two factors are equivalent for flight at sea level at the same lift coefficient. Satisfying these scaling parameters insures that, if the nondimensional aerodynamic parameters are the same for the model and full-scale airplane, the motions for a given gust angle-of-attack disturbance will be geometrically similar, the time history of load factor will be the same, and the damping ratios of transient motions will be the same. The numerical factors giving the ratios of some of the dimensional variables are shown in table I.

Model parameters.- The model's inertial parameters and loading spring gradient are compared to the scaled values of the full-scale airplanes in table I. The mass of the model was scaled approximately the same as the airplane, but the pitch inertia I_y was almost 50 percent too large. The model flap and vane inertias were about twice as large as the inertias estimated in reference 3 and about 20 percent less than the more realistic values based on an unpublished engineering design estimate. The fact that the model spring gradient is larger than the scaled airplane value used in the engineering design is not considered important. The spring was used primarily to obtain a different set of flap-response characteristics for comparison with the spring-absent data. Although the model was not in perfect scale, the model responses should be fairly representative of a full-scale light airplane with the system installed.

Mounting system.- The model was restrained in the tunnel by the dynamic rod mounting system shown schematically in figures 7 and 8. The mounting system had ball bearings placed at 90° intervals around the mounting rod. (See fig. 8.) These bearings allowed approximately 3 m of vertical travel by rolling up and down the rod, and the pitch pivot allowed about 30° freedom about the pitch axis. The model was carefully constructed and balanced so that the longitudinal and vertical coordinates of the center of gravity were nearly on the pitch pivot axis. The model could easily twist about the rod to provide yaw freedom of 360°,

but only a small fraction of this travel was used because of the directional stability of the model.

Two steel cables were attached to the bearing housing so that the model could be restrained in the middle of the tunnel before and after the tests were run. Also, two small, light nylon lines were attached to the vertical tail to restrain the model in pitch. The steel cables, the nylon lines, and the multiconductor cable shown in figure 7 trailed from the model in long loops during the dynamic tests. The influence of these cables and lines on the model was assumed to be negligible. This assumption was partially based on the fact that the larger and probably more important cables were arranged so that their resultant force passed as closely as possible to the pitch pivot axis (the center of gravity), thus minimizing the moments they produced. The resultant force produced by these cables and lines was also largely in the direction of model drag, and the model was completely restrained in that direction. Any force in the lift direction is thought to be small compared to the lift on the wing.

Controls.- The model was equipped with several different features for remotely controlling and trimming the model, at the desired test conditions, as shown in figure 7. A servocontrolled elevator was used for trimming the model in pitch, a servocontrolled vane-incidence system was used for trimming the flap, and a motor-driven screw was used to tension the loading spring. The control commands to these systems were sent from a small panel operated manually by a "pilot" in the tunnel control room while observing the model's condition. These pilot commands were sent via electrical signals through a 1-cm-diameter multiconductor cable. A light nylon line was attached to the outboard end of the vane and was used to deflect the interconnected vane-flap system for the flap-disturbance measurements.

Instrumentation.- The model was equipped with a variety of onboard instrumentation, as shown in figure 7. Two linear accelerometers, mounted fore and aft of the pitch pivot point on the model center of gravity, were used to measure the acceleration at the center of gravity by averaging the signals from both accelerometers. A pitch-rate gyro mounted forward of the center of gravity and a potentiometer attached to the mounting system were used to measure the pitch rate and pitch attitude of the model, respectively. Another potentiometer attached near the flap hinge line was used to measure the flap-vane position. The electrical power to and the response signals from the onboard sensors were sent through the multiconductor cable. The outputs of these transducers were recorded on an FM tape recorder for subsequent analysis using the real-time analyzer described in the wind-tunnel section. An oscillographic recorder was also used for the real-time recordings of the transducer outputs.

PROCEDURE

Wind-Tunnel Tests

Test conditions.- The tunnel was run using air at normal atmospheric pressure and density. The tunnel velocity was approximately 22 m/sec. This velocity was required for Froude scaling at cruise conditions. Because the TDT is a transonic facility, this velocity was below the normal operational envelope.

Consequently, the velocity could not be accurately controlled and varied as much as ±5 percent during a given run, and from run to run. The Reynolds number at the desired test condition was 0.37×10^6 based on the model wing chord.

Types of test.- Four types of tests were made. The gust-generating vanes were not used for the first three types. The first type of test was used to measure the flap response to a slowly changing angle of attack. The model was restrained in heave (steel cables in tension). The flaps were trimmed to zero deflection using the vane-incidence control. The model was then slowly pitched throughout its limit of travel using the elevator control. The pitch attitude (angle of attack) of the model was plotted against the flap deflection.

The dynamic response of the flap-vane system with the model restrained in both heave and pitch (both the steel cables and nylon lines attached to the tail in tension) was measured in the second type of test. For this test, the flap was trimmed to a zero deflection, and then the flap was deflected to its limit of travel by pulling on the light nylon line attached to the vane. The line was then released, and the resulting flap motion was recorded on the real-time oscillograph.

The purpose of the third type of test was to determine the short-period motion with the model free in both heave and pitch as in the later gust-response tests. After the model was trimmed with the tunnel running, the model was disturbed by pulling and releasing the lower of the two nylon lines attached to the vertical tail. The resulting motion was recorded on the real-time oscillograph.

The fourth type of test involved measurement of the model's response to the sinusoidal vertical gust excitation. In these tests the model was free to heave and pitch as the gust vanes were oscillated at $\pm 12^\circ$ incidence change. The frequency of the gust vane oscillation was steadily decreased (linear sweep) from a frequency of 15 to 0.5 Hz over a period of approximately 10 min. During these tests the model response to the generated gusts was recorded on the FM tape recorder for later playback into the real-time analyzer.

Experimental variables.- Three basic experimental variables were investigated during these tests. The first and most important was the gearing ratio γ, which is defined as the ratio of the change in vane dihedral angle to the resulting change in flap deflection. The second variable was the use or absence of the loading spring with its rotational spring gradient K_s. The third variable was the flap-chord length. The flap chord was extended approximately 50 percent by attaching thin strips of balsa to the upper and lower edges of the flap. More mass-balance weight was added to compensate for the added mass of the balsa strips. The balance weight was added to the vane weight instead of the flap weight for convenience so that the total system was approximately balanced.

Theoretical Analysis

The theoretical static flap gain K and the theoretical flap natural frequency $\omega_{n,f}$ and flap damping ratio ζ_f were calculated using equations (A5), (A7), and (A8) in appendix A. The values for the static aerodynamic terms $C_{h\delta_f}$,

$C_{h_{\alpha_v}}$, and $C_{h_{\alpha_f}}$ used in these equations were from unpublished wind-tunnel data on the subject model and are presented in table II. The values for the nondimensional dynamic terms $C_{h_{\delta_v}} = \dfrac{\partial C_h}{\partial\left(\dfrac{\delta_v c}{2V}\right)}$ and $C_{h_{\delta_f}} = \dfrac{\partial C_h}{\partial\left(\dfrac{\delta_f c}{2V}\right)}$ are also given in table II and were calculated using procedures in references 3 and 8, respectively.

The equations of motion used to represent the combined model-flap response were taken from reference 5 and are reproduced in appendix B. The Z-force and pitching-moment equations are based on the original analysis given in reference 9. The aerodynamic derivatives used in the equations were determined from static wind-tunnel measurements of the subject model described in reference 5 and are listed in table II. Flap equation characteristics (K, $\omega_{n,f}$, and ζ_f) were taken from the present quasi-static and dynamic flap-response tests. The actual tunnel test velocity at the time of maximum model response was used in the theoretical analysis rather than the desired velocity. The equations of motion were solved to produce the roots of the characteristic equation and the frequency response to gust angle-of-attack changes.

The two low-frequency short-period roots of the characteristic equation were used for comparison with the measured responses. The flap-response measurements were compared with calculations using equations (A7) and (A8) rather than the characteristic roots, since these measurements were made with the model restrained so that the short-period motion would not influence the measurements.

One of the primary purposes of the present tests was to determine the amount of alleviation a full-scale version of the system would produce in atmospheric turbulence based on the experimental results. The rms normal acceleration per unit of rms vertical gust velocity was taken as the measure of alleviation and was given for the full-scale airplane by

$$\frac{\sigma_n}{\sigma_{wg}} = \left\{ \int_{\Omega_1}^{\Omega_2} \left[\frac{n}{w_g}(\Omega) \right]^2 \frac{\Phi_{wg}(\Omega)}{\sigma_{wg}^2} \, d\Omega \right\}^{1/2}$$

where $\left[\dfrac{n}{w_g}(\Omega)\right]$ was the airplane response based on the experimental model results, and $\Phi_{wg}(\Omega)$ was the one-dimensional Von Karman gust spectrum for vertical gust velocities. Thus

$$\frac{\Phi_{wg}(\Omega)}{\sigma_{wg}^2} = \frac{L}{\pi} \frac{1 + \frac{8}{3}(aL\Omega)^2}{\left[1 + (aL\Omega)^2\right]^{11/6}}$$

with

$$L = 1000 \text{ m}$$

$$a = 1.339$$

$$\Omega = \omega/V$$

and

$$V = 53.64 \text{ m/sec}$$

The airplane response term $\left[\frac{n}{w_g}(\Omega)\right]$ was taken to be equal to the corresponding model response corrected for scale differences as follows: Assuming that α_g is small

$$\left[\frac{n}{w_g}(\Omega)\right]_{airplane} = \frac{1}{V}\left[\frac{n}{\alpha_g}(\Omega)\right]_{airplane}$$

Because n and α_g scale [illegible] (see table I)

$$\left[\frac{n}{\alpha_g}(\Omega)\right]_{airplane} = \left[\frac{n}{\alpha_g}(\Omega)\right]_{model}$$

Substituting this relationship in the previous one produces the scaled relationship between the airplane response and the measured model response

$$\left[\frac{n}{w_g}(\Omega)\right]_{airplane} = \frac{1}{V}\left[\frac{n}{\alpha_g}(\Omega)\right]_{model}$$

The scaling between the wave number Ω for the full-scale airplane and the experimental model frequency f can also be determined using the scale factors in table I:

$$(f)_{model} = \left(\frac{\omega}{2\pi}\right)_{model} = \left(\frac{\lambda^{-1/2}\omega}{2\pi}\right)_{airplane}$$

but

$$(\omega)_{airplane} = (V\Omega)_{airplane}$$

so that

$$(f)_{model} = \left(\frac{\lambda^{-1/2}V\Omega}{2\pi}\right)_{airplane} = \Omega\left(\frac{\lambda^{-1/2}V}{2\pi}\right)_{airplane}$$

In order to compare the experimentally "predicted" rms normal acceleration with theoretically predicted values, the theoretical model frequency responses were multiplied by the same Von Karman gust spectrum as were the experimental frequency responses. Both the experimental and theoretical rms values were further corrected for differences in model mass, model wing area, and tunnel dynamic pressures. (The theoretical calculations included all these differences.) The basic model (with vanes removed) was taken as the standard condition, and all other conditions were corrected to be comparable with this condition. The combined correction was a first-order approximation given by the following formula:

$$(\sigma_n)_{corrected} = (\sigma_n)_{uncorrected} \frac{m}{m_{basic}} \frac{S_{basic}}{S} \frac{q_{basic}}{q}$$

The combined corrections were usually small and averaged about 5 percent with a maximum of 11 percent.

RESULTS AND DISCUSSION

The following results are presented according to the type of response. There are three model configurations that are referred to in the following discussion. The "alleviated" model consists of the model with vanes installed and actively driving the flaps, as described earlier. The vanes could be removed from the model and the flaps rigidly fixed so that the model resembled an unmodified light airplane. This configuration is called the "basic" model herein and is used as the standard for comparison with the "alleviated" model. The third model configuration was the same as the "alleviated" model except both the vanes and flaps were fixed.

Data are not presented for all types of measurements for all configurations tested, but it is thought that sufficient data are presented to cover conditions of interest. The experimentally determined responses are compared with theoretical predictions in each section. It will be shown that the theory usually predicts the correct general relationship (trends) between the change in a variable and the resulting change in a response. There are significant differences, however, in the magnitude of the values of predicted and measured responses.

Quasi-Static Flap Response

The variations of flap deflection with pitch attitude (angle of attack) of the model for two particular configurations are shown in figure 9(a). (The negative of the slope of this type of plot is the static flap gain K in eq. (B3).) The data show up to 2° of hysteresis in the quasi-static response, probably due to friction in the system. There also appears to be a distinct offset in the data near a pitch attitude of zero for the condition without the spring. This offset was probably due to excessive free play in the flap-vane linkages which became apparent when the vane changed from an up to a down load. The spring, however, required the vane to have an up load at all flap deflections so that the free play was less noticeable. The offset was not readily apparent for the

extended-chord condition either, perhaps due to the imbalance of the flap because the mass balance for the flap extension was added to the vane for convenience. The hysteresis and change in free play shown in the data were not accounted for in any of the theoretical predictions of the model gust responses which are presented subsequently because a linear mathematical model was used. The marked change in slope at the limits of travel is caused by the vane or the flap hitting its stops.

A comparison of the measured slope of the curve of flap deflection against angle of attack based on equation (A5) for various configurations is given in figure 9(b). The data points are generally concentrated around the perfect agreement line. This agreement indicates that, as the gearing ratio was changed to produce the different data points, the theoretically predicted relationship between the gearing ratio and K was demonstrated experimentally.

Dynamic Flap Response

A typical time-history flap response produced by releasing the flap from the deflected position is shown in figure 10(a). The flap response is almost critically damped. Even though the model was restrained in pitch, a slight oscillation appears, but this oscillation is not considered significant. The damping and natural frequency of the flap were calculated for many different conditions from similar time-history records using the procedure in reference 10 for heavily damped second-order systems. The results of these calculations are compared to predicted damping ratios and natural frequencies in figure 10(b). (The gearing ratio γ was varied to produce the different data points for a given configuration of spring and flap chord.) The measured flap-vane damping ratios were generally greater than the predicted ones, probably because the friction in the hinges, bellcrank, and linkages was not accounted for in the theoretical predictions. The measured flap-vane natural frequencies, on the other hand, were slightly less than predicted. The damping ratios were not well correlated with the perfect agreement line, probably also because of the friction. The natural frequencies, which are probably not influenced as much by friction, however, were fairly well correlated with the perfect agreement line. This result indicates that the correct relationship between the gearing ratio and the natural frequency was demonstrated experimentally.

Short-Period Response

A typical short-period transient oscillation produced by disturbing the alleviated model in pitch is shown in figure 11(a). The damping ratios and natural frequencies of similar transient oscillations were calculated using procedures described in reference 10 for lightly damped second-order systems. The results of these calculations for different experimental conditions are shown in figure 11(b). (The gearing ratio γ was varied to produce the different data points for a given configuration of loading spring and flap chord.)

Both the measured and predicted damping ratios of the basic model (shown by the diamond-shaped symbols in fig. 11(b)) are smaller than the value of 0.8 to 1.0 obtained from unpublished flight-test data for a full-scale airplane similar

to the present model. Thus, both the predicted and measured damping ratios for the basic model and the alleviated conditions may be less than full-scale values. Larger damping ratios are desirable since reference 11 has indicated that a damping ratio of less than 0.25 may be unsatisfactory from a handling-qualities standpoint. The measured values may be low because the mounting system and the control lines and cables were influencing the model in some way.

The measured damping ratios with the alleviation system operating are less than the predicted short-period damping ratios. Both the predicted and measured short-period damping ratios for the alleviated conditions are generally less than those for the basic model, as shown in figure 11(b); therefore, the theoretical prediction that alleviation reduces the short-period damping is demonstrated experimentally. The measured natural frequency of the short period shows better agreement with the predicted values than the damping ratios. Again, the short-period frequency is generally less for the alleviated conditions than for the basic (unalleviated) condition, as predicted by theory.

Vertical-Gust Excitation Response

Time-history representation.- Time histories of the responses of the basic model and the alleviated model during a sweep of the gust-generating vanes are shown in figure 12. The frequency of gust vanes was approximately 5.0 Hz at the beginning of the record and 0.5 Hz at the end of the record. The large, low-frequency oscillation in the pitch and other responses is typical of the occasional pilot-control maneuvers used to maintain the model near the middle of the tunnel. The higher-frequency responses are due to the gusts generated by the tunnel vanes and contain the information of interest. These responses are approximately sine waves of the same frequency as the gust-generating vanes, thus indicating the response being measured is not a transient response; that is, the sweep rate of gust vanes was slow enough so that a good approximation of the frequency response of the model was obtained.

The envelopes of the responses at the beginning of the record (high frequency) are small because the gusts generated by the vanes at high frequency are very small. (See fig. 4.) As the frequency decreases, the magnitude of the responses grows larger and reaches a maximum near a frequency close to the model's short-period frequency.

Frequency-domain representation.- The time histories recorded on the FM tape recorder were played back into the real-time analyzer using the peak-hold mode described in the section on wind-tunnel calibration. The results of this data-reduction procedure for the time histories shown in figure 12 are presented in figure 13. It is apparent from the figure that the alleviated condition had less normal-acceleration response and more pitch response than did the basic model with flaps fixed. The increased pitching response is due to the pitching moments introduced by the flaps (from the change in effective wing camber and downwash on the horizontal tail) and confirms the theoretical predictions of references 3, 4, and 5. The flap response shows a symmetrical peak near the short-period frequency for the alleviated condition.

Frequency-response representation.- The frequency-response representation was calculated by taking a response amplitude in figure 13 at a given frequency and dividing it by the least-squares approximation of the gust-angle amplitude in figure 4 at the same frequency. This procedure was repeated at several frequencies from 0.5 to 4 Hz in order to describe the frequency-response curve. The calculations were not made for frequencies above 4 Hz because the gust angle was very small at higher frequencies, and the resulting accuracy of the calculations deteriorated.

The results of these calculations are shown in figure 14. The shapes of the response curves have changed, reflecting the gust-angle's functional dependence on frequency. The ratio of flap amplitude to gust amplitude shows a peak value which is much higher than the quasi-statically measured ratio of flap deflection to angle of attack (only 2.8 for this configuration). This result confirms the prediction of reference 5 and is significant because it shows the limitation of the system in alleviating large gusts without the flaps hitting the mechanical stops at the limit of the flap travel. Because the peak dynamic flap response for 1° of gust angle is more than twice as large as the quasi-static flap deflection, the system will be able to provide linear alleviation of gusts less than one-half the magnitude that might be inferred from the quasi-static response.

Agreement with theory.- A comparison of predicted and measured frequency responses is shown in figure 15. For a relatively large gearing ratio $\gamma = 0.691$ (fig. 15(a)) the predicted flap response and pitching response were about one-half of that measured. The predicted normal-acceleration response was in much better agreement. In figure 15(b) ($\gamma = 0.516$) the agreement between the predicted and the measured pitching and flapping response is somewhat better, even though the predicted responses were still less than the measured responses. The agreement for the normal-acceleration response, on the other hand, is not as good as that for the previous condition above the "knee" of the curve which occurs near the short-period frequency. The overall agreement is probably better for this case than for the first case, however.

It is believed that the agreement is better for two reasons: (1) using a spring reduced the nonlinearity in the static flap response, as shown in figure 9, and (2) the flap response was less than one-half that of figure 15(a) because of the lower gearing ratio and the use of the loading spring. The nonlinearities in the basic aerodynamic characteristics of the flap and vane were thus reduced because of the smaller flap deflections.

It should be noted that the disagreement between the predicted results and the experimental results is even greater than that predicted by the uncertainty in the statically measured aerodynamic derivatives, as discussed in reference 5. Part of this increase in the discrepancy is thought to be due to the experimental variations caused by changes in tunnel speed, uncertainty in the actual gust angle, and variation of the friction in the flap-vane system. It is possible that, with extreme care in the model building and in the test measurements, both static and dynamic, these discrepancies could be reduced. Until it can be demonstrated that the discrepancy can be reduced in this manner, however, dynamic tests must be made to verify theoretical predictions.

Experimentally Estimated Full-Scale Airplane Response to Atmospheric Turbulence

Power spectra.- The experimentally estimated normal-acceleration power spectra (for the same two experimental conditions as in figs. 12, 13, and 14) are shown in figure 16. The difference in the levels of the basic and alleviated conditions is larger in this figure than in figure 13 because the levels are proportional to the amplitude squared. The shape of the curves is also different because the model response is to the Von Karman gust spectrum rather than the TDT gust spectrum.

Amount of alleviation.- The normalized rms normal-acceleration responses to atmospheric turbulence for several different conditions are shown in figure 17 as a function of flap-vane gearing ratio. These values are equal to the square root of the area under curves such as those in figure 16. Even though the areas are over only a restricted range of frequency, they should contain most of the power which would be contained if all frequencies were included; that is, the frequency range includes the region around the short-period frequency which contains most of the power (see the large-frequency-range power spectra in ref. 3). That most of the power is in the region of the short-period frequency is especially true if the reasonable assumption is made that the pilot would damp out the low-frequency phugoid response.

As shown in appendix A, increasing the gearing ratio causes the static alleviation factor to increase, the flap natural frequency to decrease, and the flap damping ratio to increase. The theoretical relationship among these three factors is slightly different for each of the three combinations of flap chord and loading spring tested. As shown in reference 5, increasing that static alleviation factor increases the alleviation up to a theoretical optimum alleviation factor of 0.75 if the flap-response characteristics are assumed constant. It was also shown that reducing the flap damping ratio above about 0.25 reduces the amount of alleviation. There are, therefore, conflicting theoretical trends as the gearing ratio is increased, and a static alleviation factor of less than 0.75 might be expected to be optimum. The actual optimum gearing ratio (static alleviation factor) is a complex function of the flap-vane aerodynamic and inertial characteristics and airplane or model characteristics.

Although there is some scatter in the data, there seems to be a minimum at an approximate gearing ratio of 0.5 for the nominal alleviated condition ($K_s = 0$ and $c_f = 0.068$ m). The optimum experimental alleviation achieved was about 30 percent for this configuration. The experimentally determined optimum gearing ratio of 0.5 corresponds to a calculated static alleviation factor of 0.41 so that the optimum occurred at a nonzero effective lift-curve slope as predicted by theory (ref. 5). The theoretically predicted optimum point seems to be at a slightly higher gearing ratio or a higher static alleviation factor, although the theoretical curve is nearly flat in the region. At low gearing ratios (≈ 0.2) the experimental alleviation is less than the theoretical probably because break-out friction is more dominant at low gearing ratios. The theoretically predicted response of the basic unalleviated airplane is practically the same as that predicted experimentally.

The spring-on data (K_s = -0.23 N-m/rad and c_f = 0.068 m) show an optimum level at a higher mechanical gain than that of the spring-off case (K_s = 0 and c_f = 0.068 m). There appears to be slightly less rms alleviation (more response) with the spring on than with the spring off, although the difference may be within the accuracy of the measurements. Theoretically, the alleviation should be about the same because the static alleviation factor and the flap natural frequency were about the same. However, the loading effect of the spring on the flap bearings and the horizontal gust-alleviation capability of the spring may have caused some differences in the response.

Only two gearing ratios were tested for the extended-flap-chord condition. For the higher gearing ratio, the alleviation achieved was as good or better than that achieved for the shorter-chord conditions, that is, about 40 percent. The present alleviation was achieved in spite of the fact that the calculated flap natural frequency was practically one-half that of the shorter-chord optimum conditions. As shown in reference 5, the shorter-chord flap should be superior to the longer-chord flap because of the increased natural frequency. This seemingly contradictory result, however, is not firmly established because of the small amount of data obtained. Further tests are needed to establish the relationship between flap chord and alleviation. It is possible that the pitching-moment characteristics of an extended-chord flap are favorable and that this effect outweighs the effect of the reduced natural frequency of the flap-vane system.

CONCLUDING REMARKS

Dynamic wind-tunnel tests have been made of a 1/6-scale model of a general-aviation airplane equipped with an aeromechanical gust-alleviation system. Experimental results have been compared with theoretical predictions of the mathematical model of reference 5 using statically determined aerodynamic characteristics and dynamically measured flap-response characteristics. The experimental results included the normal-acceleration, pitching, and flapping responses to external disturbances and to sinusoidally varying gust disturbances in the longitudinal short-period frequency range.

The mathematical model usually predicted the correct relationship between a change in a given variable and the resulting change in the response but did not accurately predict the absolute level of response. These discrepancies were too large to be accounted for by the uncertainty in the statically measured aerodynamic characteristics. Until better agreement is obtained between the experimental and the theoretical, dynamic tests probably should be conducted to verify theoretical predictions.

Specific conclusions and results are as follows:

(1) An averaged value for the rms alleviation in normal acceleration for the best configuration was 30 percent. This value was predicted for the full-scale airplane in atmospheric turbulence based on the experimental model results over the frequency range investigated. This frequency range was thought to contain most of the power in a practical situation.

(2) The flap response to quasi-static angle-of-attack changes was in general agreement with theoretical predictions.

(3) The flap damping ratio and natural frequency were greater and less, respectively, than theoretically predicted.

(4) The short-period frequency and damping were reduced for alleviated configurations as compared with the unalleviated configuration, as was predicted theoretically. The measured short-period damping ratio was substantially less than theoretically predicted, however.

(5) The normal-acceleration response to gusts was reduced and the accompanying pitching response was increased for alleviated configurations compared with the unalleviated configuration.

(6) The dynamic flapping response to gusts was much larger than the quasi-static flap response. This result was predicted theoretically.

(7) The measured flapping and pitching responses to gusts were larger than theoretically predicted, although the discrepancy was reduced for smaller values of the static alleviation factor.

(8) Extending the flap chord 50 percent produced as good or better alleviation than the nominal shorter-chord condition. Theory would predict a decrease in alleviation due to the lowered flap-vane natural frequency.

Langley Research Center
National Aeronautics and Space Administration
Hampton, VA 23665
July 13, 1977

APPENDIX A

ANALYSIS OF THE EFFECT OF THE MECHANICAL GEARING RATIO AND LOADING SPRING GRADIENT ON THE STATIC ALLEVIATION FACTOR, FLAP NATURAL FREQUENCY, AND DAMPING RATIO

The equation for the hinge moment about the flap hinge line is given in reference 5 and repeated here

$$H = \ddot{\delta}_f(I_f + \gamma^2 I_v) = \delta_f\left[\left(\frac{1}{2}\rho V^2 S_f c_f\right)\left(\frac{c}{2V}\right)\left(\gamma^2 C_{h\dot{\delta}_v} + C_{h\dot{\delta}_f}\right)\right]$$

$$+ \delta_f\left(\frac{1}{2}\rho V^2 S_f c_f C_{h\delta_f} + K_s\right) + \left(\frac{1}{2}\rho V^2 S_f c_f \gamma C_{h\alpha_v}\right)\alpha_v$$

$$+ \left(\frac{1}{2}\rho V^2 S_f c_f C_{h\alpha_f}\right)\alpha + (-I_f)\ddot{\theta} + K_o \tag{A1}$$

where

$$\alpha = \alpha_{trim} + \alpha_o + \alpha_g \tag{A2}$$

$$\alpha_v = \alpha + \frac{l_v\dot{\theta}}{V} + i \tag{A3}$$

This equation is equivalent to the simplified second-order form

$$\left(K\omega_{n,f}^2\right)\bar{\alpha}_o + \left(i_r s^2 - sK\omega_{n,f}^2\frac{l_n}{V}\right)\bar{\theta} + \left[\left(s^2 + 2\zeta\omega_{n,f}s + \omega_{n,f}^2\right)\right]\bar{\delta}_f = \left(-K\omega_{n,f}^2\right)\bar{\alpha}_g \tag{A4}$$

where

$$K = \frac{\frac{1}{2}\rho V^2 S_f c_f\left(\gamma C_{h\alpha_v} + C_{h\alpha_f}\right)}{\frac{1}{2}\rho V^2 S_f c_f C_{h\delta_f} + K_s} \equiv K_v\left(\frac{C_{Z_\alpha}}{C_{Z_{\delta_f}}}\right) \tag{A5}$$

$$K_v = K\left(\frac{C_{Z\delta_f}}{C_{Z\alpha}}\right) = \left(\frac{C_{Z\delta_f}}{C_{Z\alpha}}\right)\frac{\frac{1}{2}\rho V^2 S_f c_f\left(\gamma C_{h_{\alpha_v}} + C_{h_{\alpha_f}}\right)}{\frac{1}{2}\rho V^2 S_f c_f C_{h\delta_f} + K_s} \tag{A6}$$

$$\omega_{n,f} = \sqrt{\frac{-\left(\frac{1}{2}\rho V^2 S_f c_f C_{h\delta_f} + K_s\right)}{I_f + I_v\gamma^2}} \tag{A7}$$

$$\zeta_f = -\left(\gamma^2 C_{h\dot{\delta}_v} + C_{h\dot{\delta}_f}\right)\left(\frac{c}{2V}\right)\frac{\frac{1}{2}\rho V^2 S_f c_f \Big/ (I_f + \gamma^2 I_v)}{2\omega_{n,f}} \tag{A8}$$

$$i_f = \frac{I_f}{I_f + \gamma^2 I_v} \tag{A9}$$

$$l_n = \frac{l_v}{\left(\gamma C_{h\alpha_v} + C_{h\alpha_f}\right)\Big/\gamma C_{h\alpha_v}} \tag{A10}$$

The static vertical alleviation factor K_v is zero for no alleviation and one for full static alleviation. The effective lift-curve slope is zero for full static alleviation as shown in appendix A of reference 5.

The theoretical variation of K_v, $\omega_{n,f}$, and ζ_f with the gearing ratio γ is shown in figure A1 for two experimental model conditions. The model characteristics used in the calculations are those listed in table II. As the gearing ratio increases, the static vertical alleviation factor K_v and the flap damping ratio ζ_f increase while the flap natural frequency $\omega_{n,f}$ decreases.

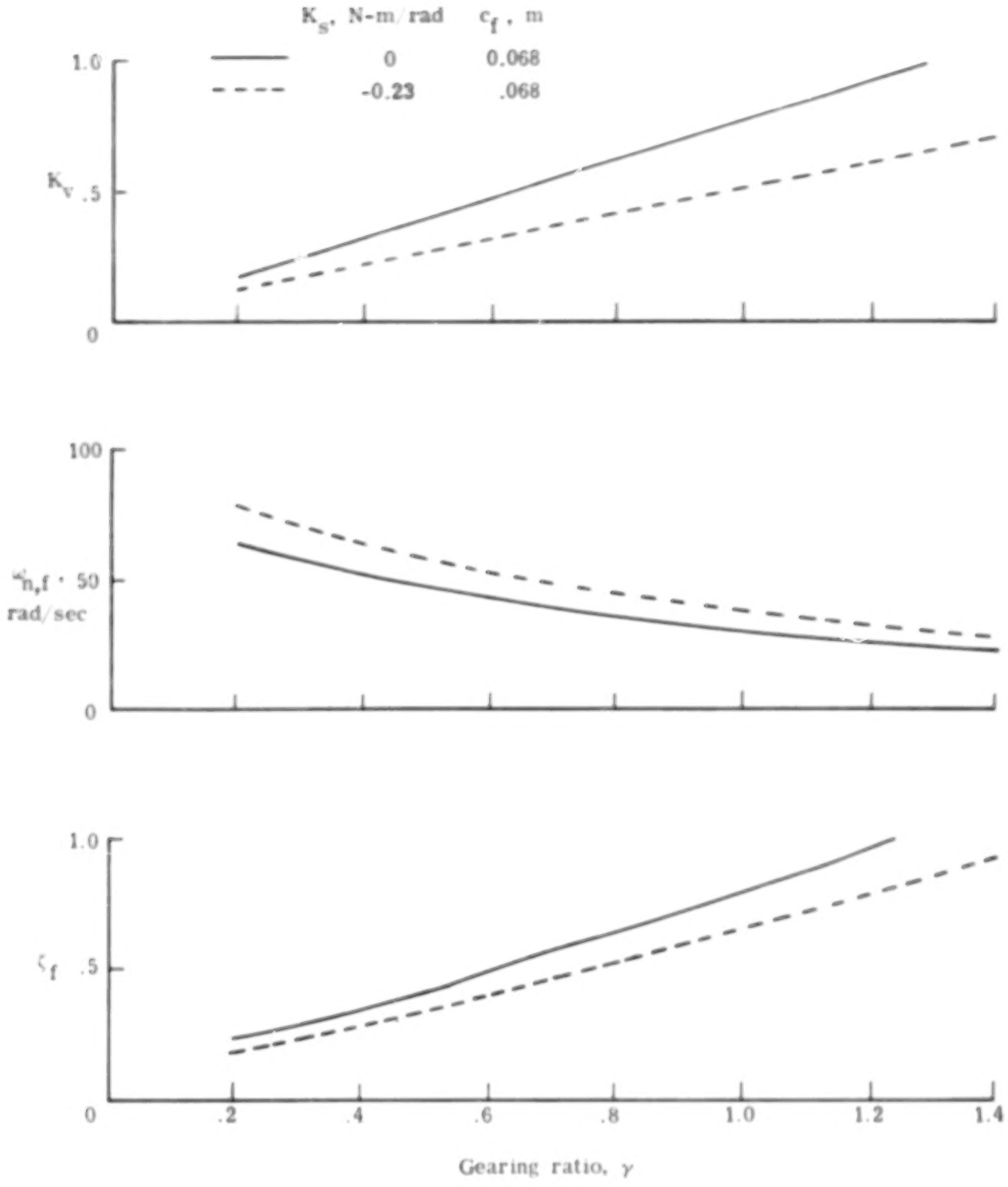

Figure A1.- Calculated flap-vane response characteristics for experimental model.

APPENDIX B

EQUATIONS OF MOTION USED IN THE THEORETICAL PREDICTION OF MODEL RESPONSE TO GUSTS

The equations of motion used herein are taken directly from reference 5. They are repeated here for convenience:

$$\left[\frac{c}{V}s\left(-2\mu + \frac{\partial\epsilon}{\partial\alpha}\ell C_{Z_{\alpha_t}}\right) + \left(C_{Z_{\alpha_w}} + C_{Z_{\alpha_t}} - \frac{\partial\epsilon}{\partial\alpha}C_{Z_{\alpha_t}}\right)\right]\bar{\alpha}_o + \left[s\frac{c}{V}\left(2\mu + \ell C_{Z_{\alpha_t}}\right)\right]\bar{\theta}$$

$$+ \left\{s\frac{c}{V}\left(\frac{\partial\epsilon}{\partial\delta_f}C_{Z_{\alpha_t}}\ell\right) + \left[-\frac{\partial\epsilon}{\partial\delta_f}C_{Z_{\alpha_t}} + \left(C_{Z\delta_f}\right)_w\right]\right\}\bar{\delta}_f$$

$$= \left[\frac{c}{V}s\left(\ell C_{Z_{\alpha_t}} - \frac{\partial\epsilon}{\partial\alpha}\ell C_{Z_{\alpha_t}}\right) + \left(-C_{Z_{\alpha_w}} - C_{Z_{\alpha_t}} + \frac{\partial\epsilon}{\partial\alpha}C_{Z_{\alpha_t}}\right)\right]\bar{\alpha}_g \qquad \text{(B1)}$$

$$\left[\frac{c}{V}s\left(\frac{\partial\epsilon}{\partial\alpha}\ell C_{m_{\alpha_t}}\right) + \left(C_{m_{\alpha_w}} + C_{m_{\alpha_t}} - \frac{\partial\epsilon}{\partial\alpha}C_{m_{\alpha_t}}\right)\right]\bar{\alpha}_o + \left[\left(\frac{c}{V}\right)^2 s^2\left(-2\mu K_y{}^2\right) + \frac{c}{V}s\left(\ell C_{m_{\alpha_t}}\right)\right]\bar{\theta}$$

$$+ \left\{\frac{c}{V}s\left(\frac{\partial\epsilon}{\partial\delta_f}\ell C_{m_{\alpha_t}}\right) + \left[-\frac{\partial\epsilon}{\partial\delta_f}C_{m_{\alpha_t}} + \left(C_{m\delta_f}\right)_w\right]\right\}\bar{\delta}_f$$

$$= \left[\frac{c}{V}s\left(\ell C_{m_{\alpha_t}} - \frac{\partial\epsilon}{\partial\alpha}\ell C_{m_{\alpha_t}}\right) + \left(-C_{m_{\alpha_w}} - C_{m_{\alpha_t}} + \frac{\partial\epsilon}{\partial\alpha}C_{m_{\alpha_t}}\right)\right]\bar{\alpha}_g \qquad \text{(B2)}$$

$$(K\omega_{n,f}{}^2)\bar{\alpha}_o + \left(i_r s^2 - K\omega_{n,f}{}^2\frac{l_n}{V}s\right)\bar{\theta} + (s^2 + 2\zeta\omega_{n,f}s + \omega_{n,f}{}^2)\bar{\delta}_f = (-K\omega_{n,f}{}^2)\bar{\alpha}_g$$

(B3)

$$\bar{n} = \frac{V}{g}s(\bar{\alpha}_o - \bar{\theta}) \qquad \text{(B4)}$$

REFERENCES

1. Hirsch, R.: L'Absorption des Rafales sur Avions et Résultats des Essais en Vol d'un Appareil Expérimental. Doc-Air-Espace, no. 105, July 1967, pp. 41-56.

2. Hewes, Donald E.; and Stewart, Eric C.: Exploratory Tests of a Simple Aero-Mechanical Ride Comfort System for Lightly Loaded Aircraft. NASA TM X-71921, 1974.

3. Roesch, Phillippe; and Harlan, Raymond B.: A Passive Gust Alleviation System for a Light Aircraft. NASA CR-2605, 1975.

4. Stewart, Eric C.: Discussion of an Aeromechanical Gust Alleviation System to Improve the Ride Comfort of Light Airplanes. [Preprint] 750544, Soc. Automot. Eng., Apr. 1975.

5. Stewart, Eric C.: An Analytical Study and Wind-Tunnel Tests of an Aeromechanical Gust-Alleviation System for a Light Airplane. NASA TN D-8234, 1976.

6. Gilman, Jean, Jr.; and Bennett, Robert M.: A Wind-Tunnel Technique for Measuring Frequency-Response Functions for Gust Load Analyses. J. of Aircraft, vol. 3, no. 6, Nov.-Dec. 1966, pp. 535-540.

7. Doggett, Robert V., Jr.; Abel, Irving; and Ruhlin, Charles L.: Some Experiences Using Wind-Tunnel Models in Active Control Studies. Advanced Control Technology and Its Potential for Future Transport Aircraft, NASA TM X-3409, 1976, pp. 831-892.

8. Küssner, H. G.; and Schwartz, L.: The Oscillating Wing With Aerodynamically Balanced Elevator. NACA TM 991, 1941.

9. Phillips, William H.; and Kraft, Christopher C., Jr.: Theoretical Study of Some Methods for Increasing the Smoothness of Flight Through Rough Air. NACA TN 2416, 1951.

10. Langdon, S. D.; and Cross, W. V.: Fixed Wing Stability and Control Theory and Flight Test Techniques - Flight Test Manual. USNTPS-FTM-103, U.S. Navy, Jan. 1, 1975. (Available from DDC as AD A023 056.)

11. Ellis, David R.: Flying Qualities of Small General Aviation Airplanes. Part 4 - Review of Recent In-Flight Simulation Experiments and Some Suggested Criteria. Rep. No. FAA-RD-71-118, Oct. 1972. (Available from DDC as AD 739 880.)

TABLE I.- MODEL CHARACTERISTICS AND TEST VELOCITY COMPARED WITH FULL-SCALE VALUES; SCALE FACTORS FOR MODEL-RESPONSE MEASUREMENTS

[The geometric scale factor is $\lambda = 0.1667$]

Model characteristics and test velocity				
Parameter	Parameter scale factor	Numerical value of parameter scale factor	Model value	Airplane value (scaled to model size)
m, kg	λ^3	4.63×10^{-3}	[a]4.87	4.83
I_y, kg-m^2	λ^5	1.29×10^{-4}	.34	.23
I_r, kg-m^2	λ^5	1.29×10^{-4}	1.31×10^{-4}	[b].36 $\times 10^{-4}$ [c].94 $\times 10^{-4}$
I_v, kg-m^2	λ^5	1.29×10^{-4}	5.04×10^{-4}	[b]2.94 $\times 10^{-4}$ [c]7.24 $\times 10^{-4}$
K_s, N-m/rad	λ^4	7.73×10^{-4}	-.23	[d]-.07 to -.15
V, m/sec	$\lambda^{1/2}$	4.08×10^{-1}	22.0	[e]22.0

Model response scale factors		
Parameter	Parameter scale factor	Numerical value of parameter scale factor
t, sec	$\lambda^{1/2}$	0.408
f, Hz	$\lambda^{-1/2}$	2.45
θ, rad	1.0	1.0
$\dot{\theta}$, rad/sec	$\lambda^{-1/2}$	2.45
δ_r, rad	1.0	1.0
n, g units	1.0	1.0
α_g, rad	1.0	1.0

[a]5.13 kg with gust-alleviation system installed.

[b]Estimated in reference 3.

[c]Unpublished estimates based on a detailed engineering design of a research version of the system.

[d]Spring gradient used in engineering design.

[e]Approximate cruise velocity.

TABLE II.- MODEL CHARACTERISTICS USED IN THEORETICAL ANALYSIS

S, m^2	0.452
S_f (both flaps), m^2	0.0512
c, m	0.247
c_f, m	0.0676
$C_{m_{\alpha_t}}$	-1.948
$C_{m_{\alpha_w}}$	0.203
$C_{Z_{\alpha_t}}$	-0.664
$C_{Z_{\alpha_w}}$ for vanes off	-4.765
$C_{Z_{\alpha_w}}$ for vanes on	-4.901
$\left(C_{m_{\delta_f}}\right)_w$	-0.164
$\left(C_{Z_{\delta_f}}\right)_w$	-1.073
$\partial\epsilon/\partial\alpha$	0.276
$\partial\epsilon/\partial\delta_f$	0.098
l	2.934
l_n	0
$C_{h_{\alpha_f}}$	-0.065
$C_{h_{\alpha_v}}$	-2.28
$^{*}C_{h_{\delta_f}}$	-0.57
$C_{h_{\dot{\delta}_f}}$	-0.64
$C_{h_{\delta_v}}$	-5.61

$^{*}C_{h_{\delta_f}}$ used in the calculations for figure 9(b) for the extended-flap-chord condition was assumed to be equal to $(1.50)^2 C_{h_{\delta_f}}$ for the basic flap chord listed herein.

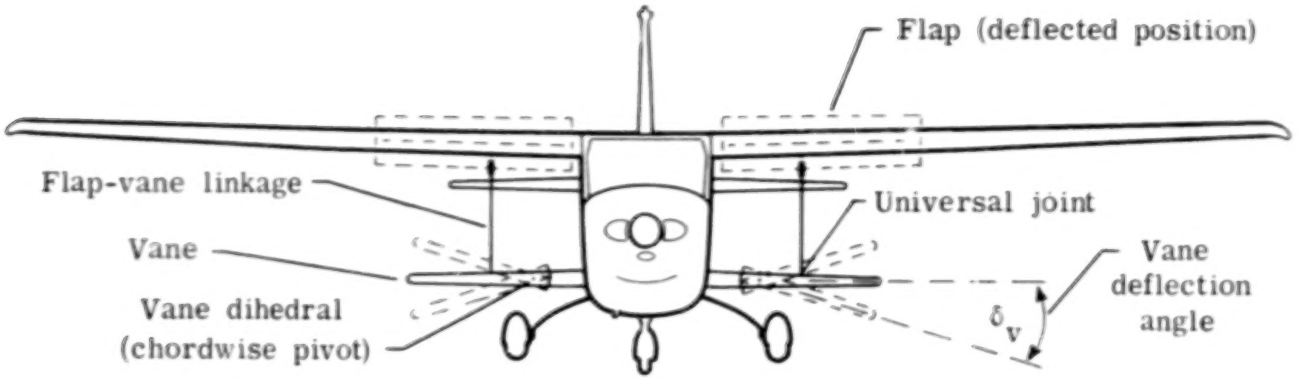

(a) Front view (flaps and vanes shown in deflected positions by dashed lines).

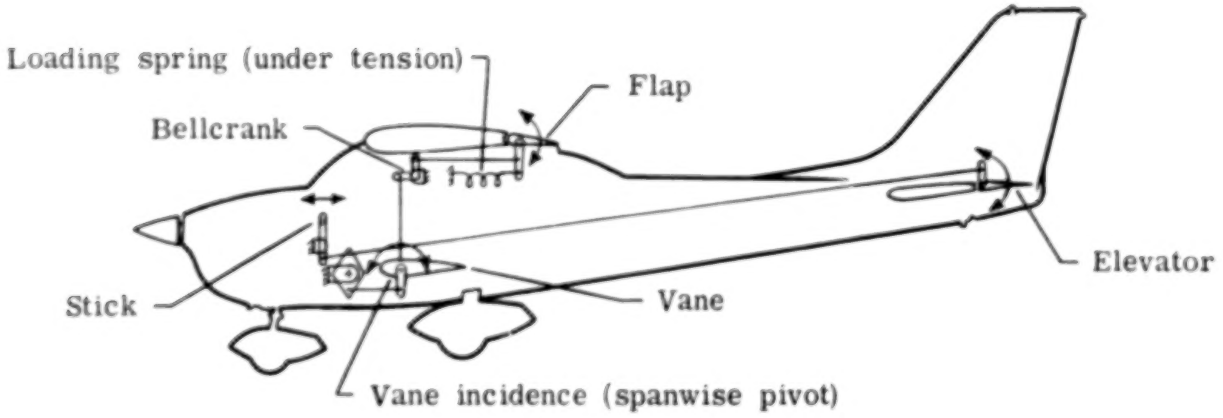

(b) Side view (flap and vane shown in neutral position).

Figure 1.- Schematic representation of gust-alleviation system.

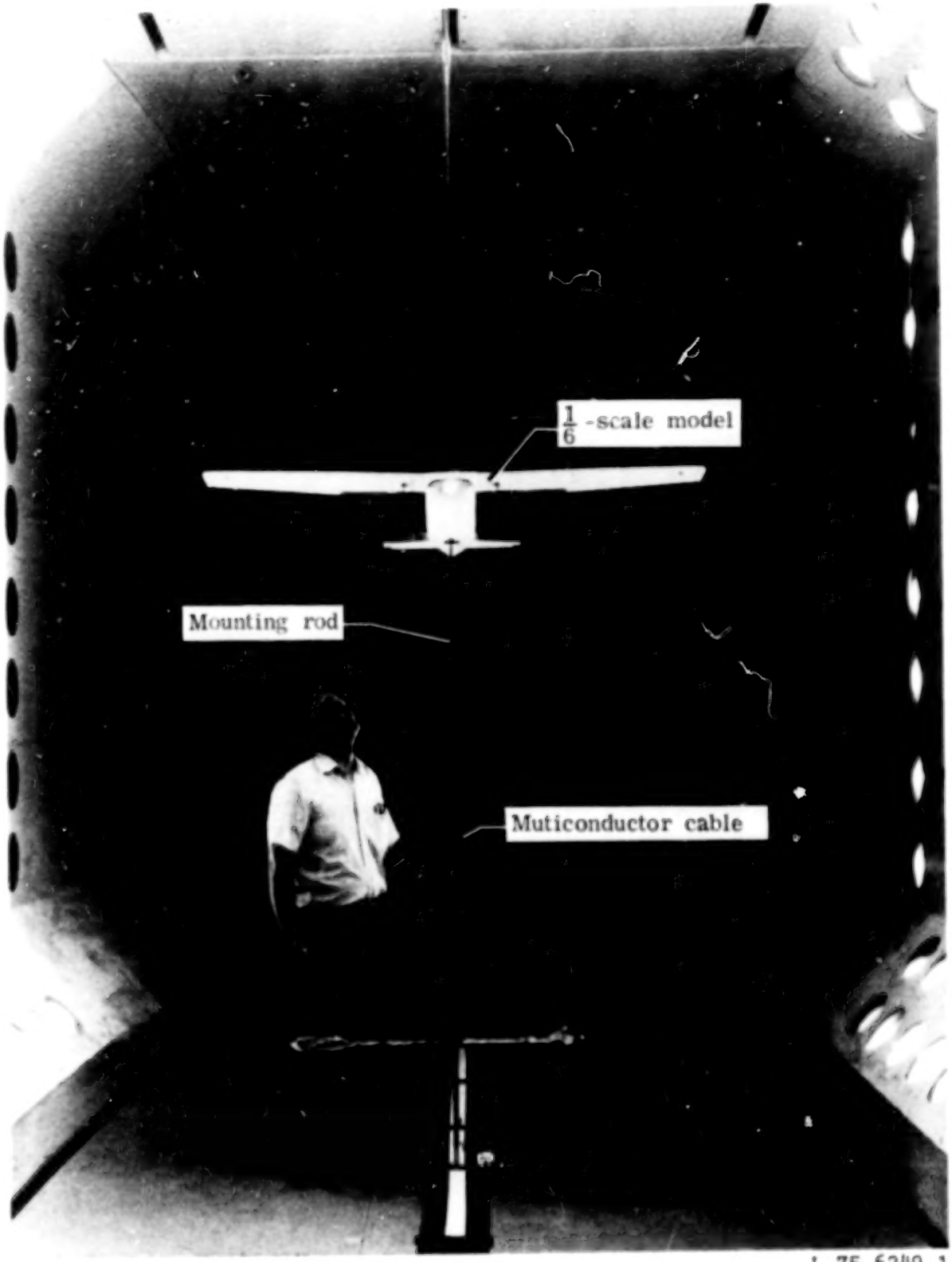

L-75-6249.1

Figure 2.- The 1/6-scale model mounted in test section of Langley transonic dynamics tunnel (TDT).

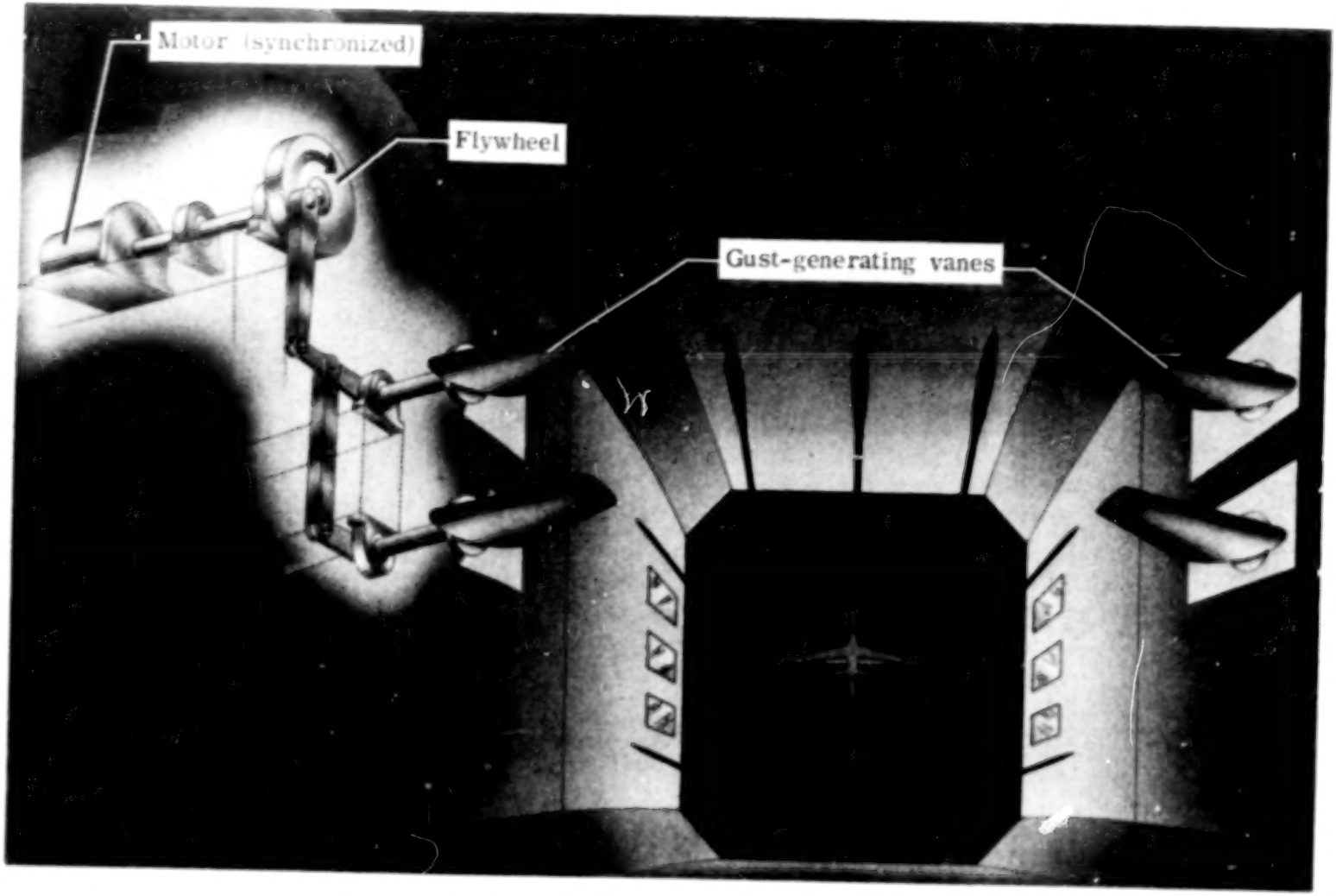

L-77-252

Figure 3.- Sketch of airstream oscillator vanes and model, with cutaway showing schematic of mechanism.

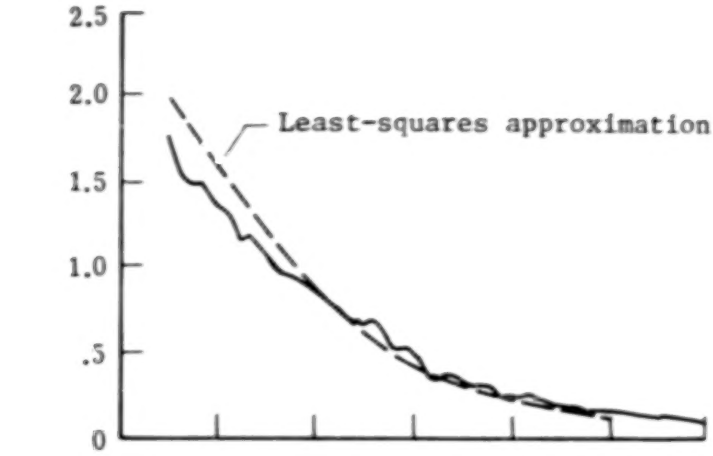

(a) Gust angle 0.91 m above centerline.

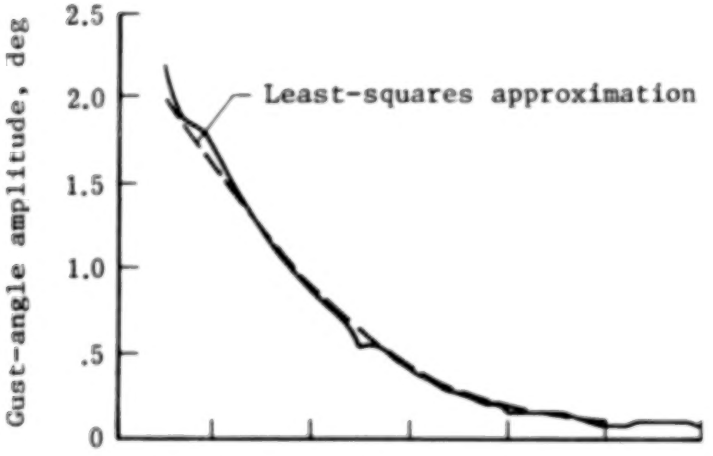

(b) Gust angle on centerline.

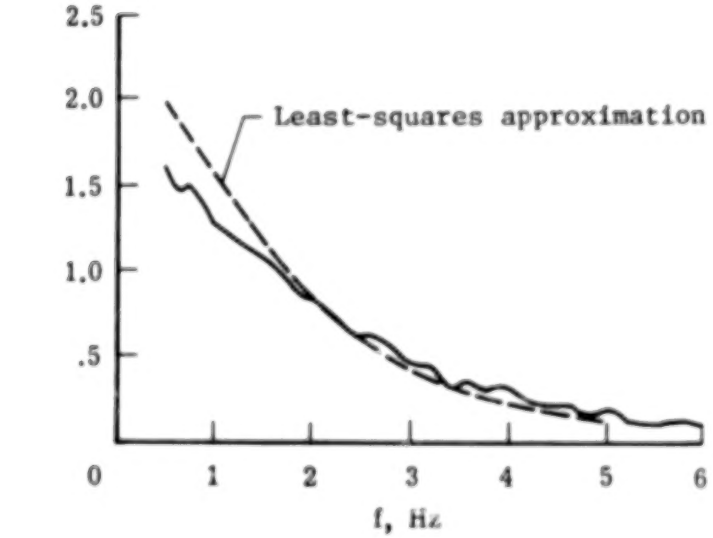

(c) Gust angle 0.91 m below centerline.

Figure 4.- Gust angle produced by oscillating gust vanes in Langley transonic dynamics tunnel.

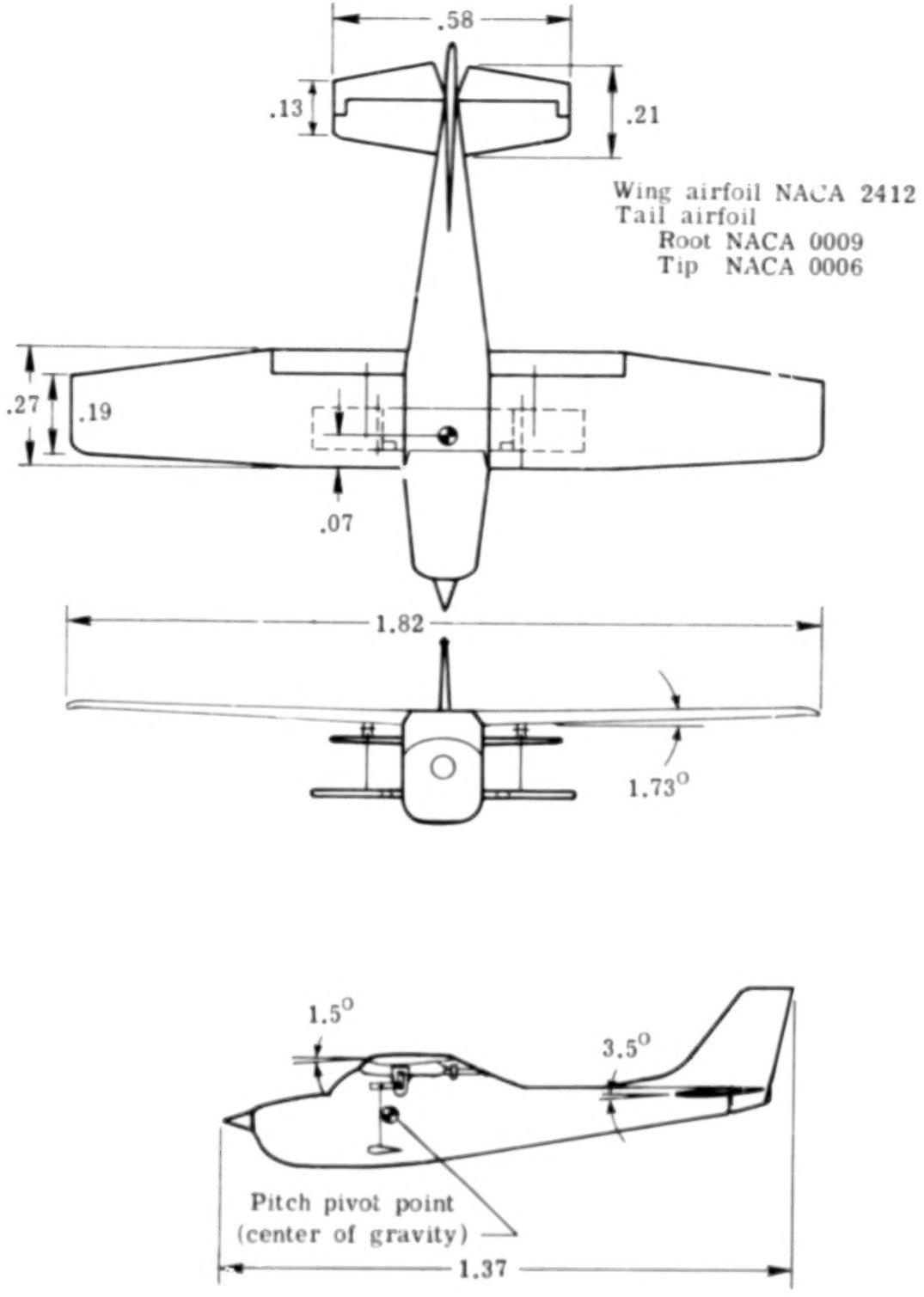

(a) Three-view drawing of model. (All dimensions are in m.)

Figure 5.- Three-view drawing of model with detailed views of vane and flap.

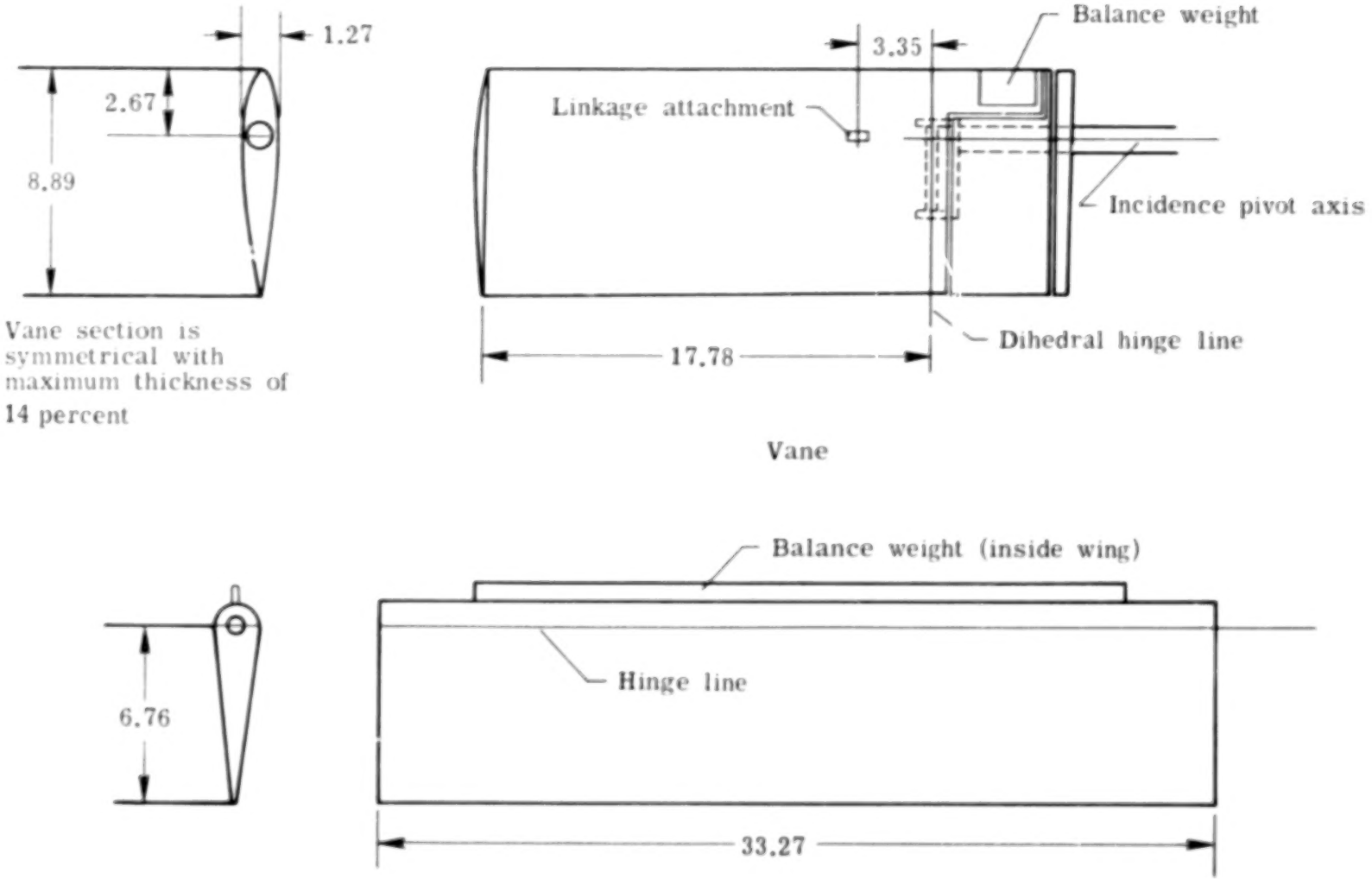

(b) Detailed views of vane and flap. (All dimensions are in cm.)

Figure 5.- Concluded.

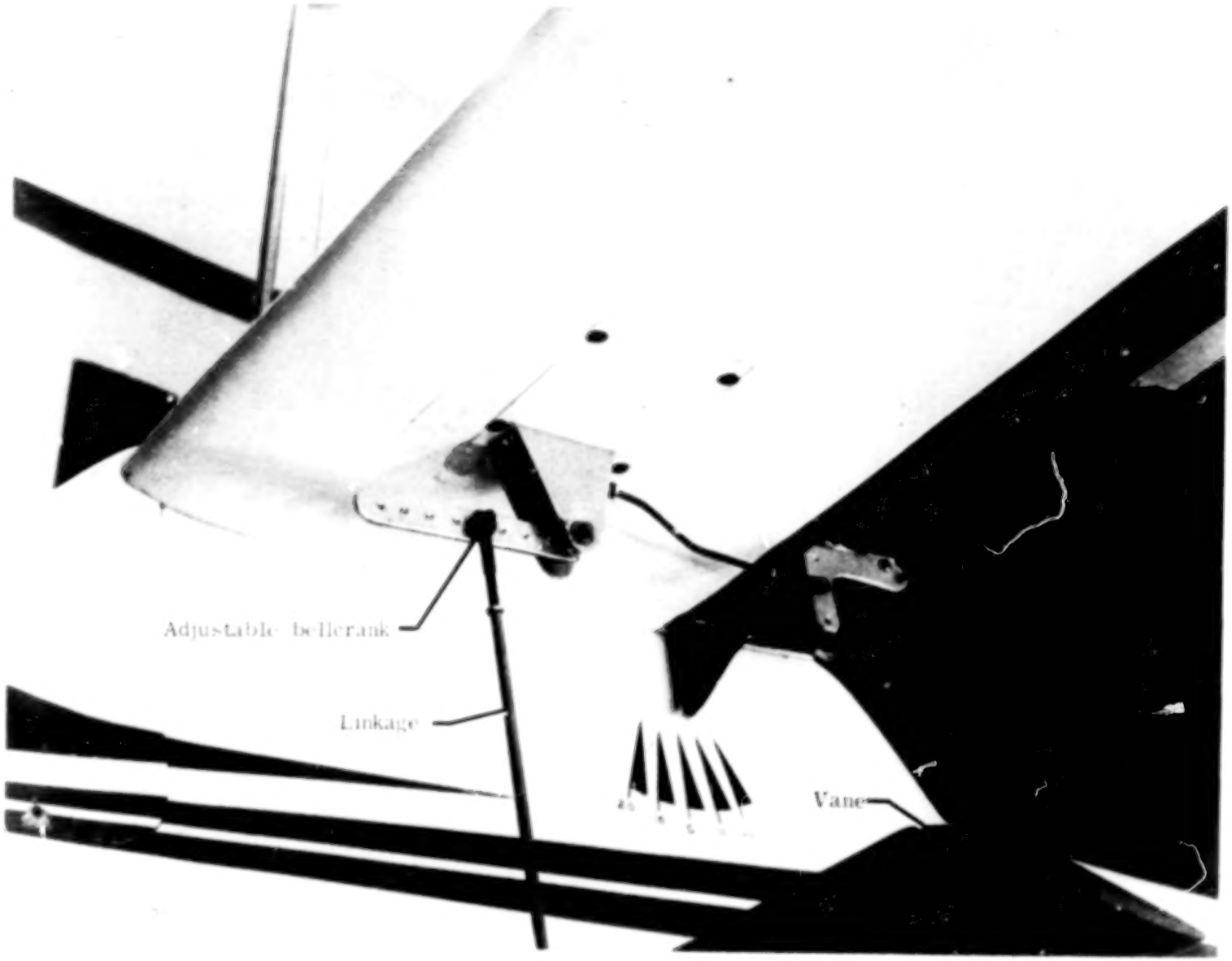

L-77-253

Figure 6.- Photograph of flap-vane linkages and bellcrank system showing holes used to vary flap-vane gearing ratio.

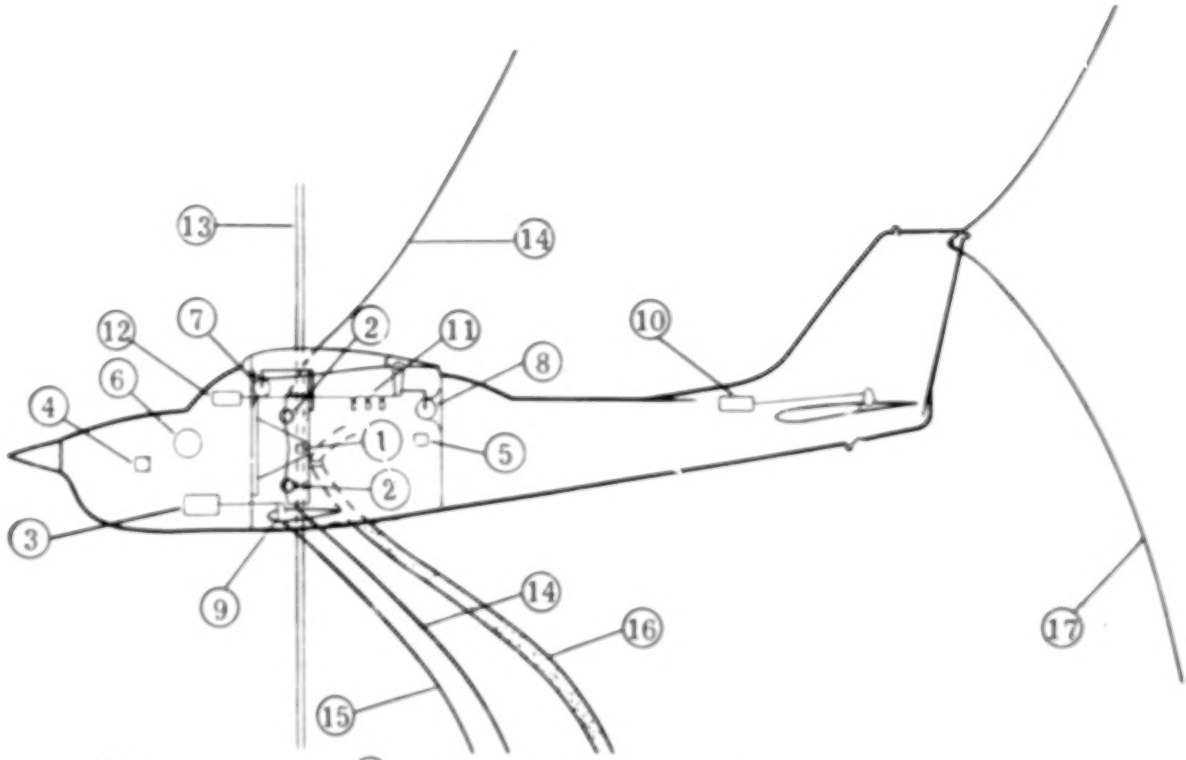

Key

1. Pitch pivot axis
2. Ball bearings
3. Vane-incidence servo
4. Forward accelerometer
5. Aft accelerometer
6. Pitch-rate gyro
7. Pitch-attitude potentiometer
8. Flap-position potentiometer
9. Vane-incidence pivot axis
10. Elevator servo
11. Loading spring
12. Motor for tensioning loading spring
13. 6.35-mm steel rod held in tension
14. 1.59-mm flexible steel cable for heave restraint
15. Nylon line for flap-vane deflection
16. 1-cm multiconductor cable
17. Nylon line for pitch restraint

Figure 7.- Schematic representation of model's instrumentation arrangement.

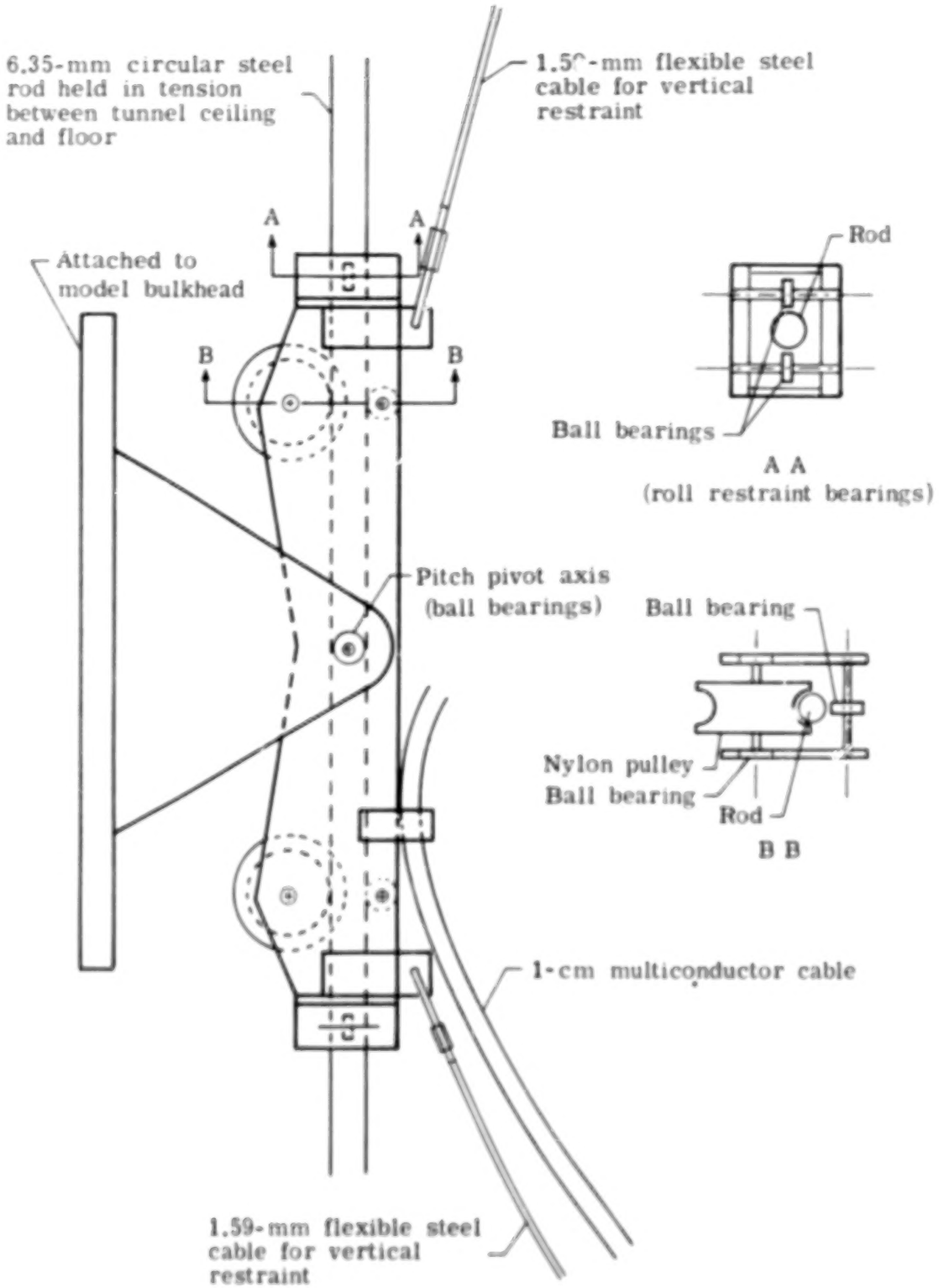

Figure 8.- Dynamic mounting system used to allow model vertical, pitch, and yaw freedom.

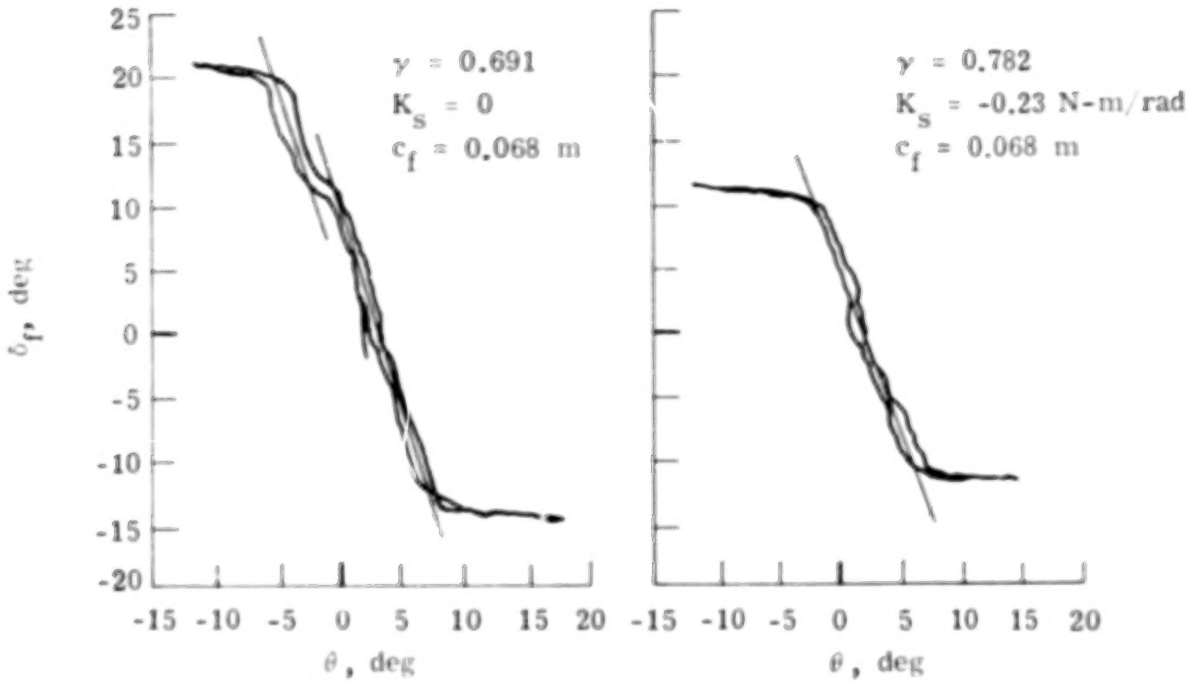

(a) Typical quasi-static flap response.

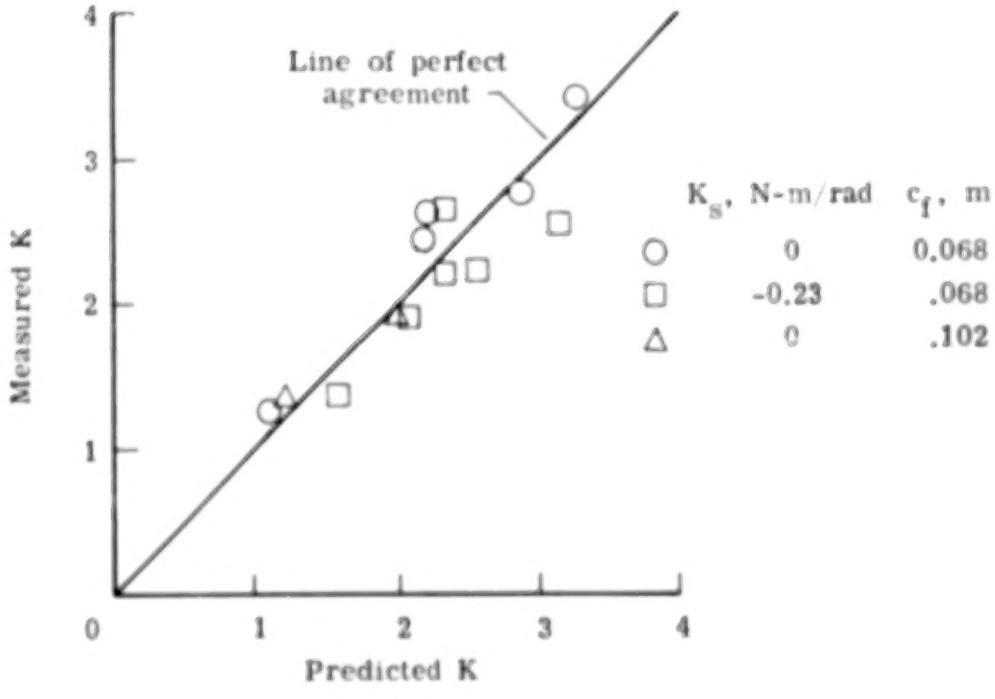

(b) Negative of slope of quasi-static flap response, K.

Figure 9.- Quasi-static flap response to angle-of-attack changes with model restrained in heave.

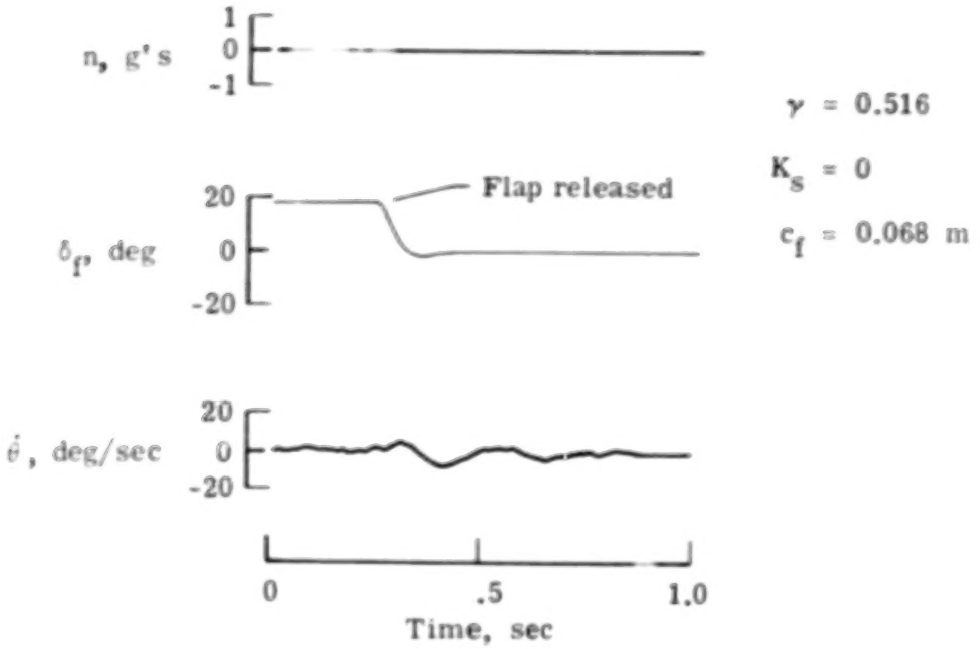

(a) Typical time history of flap response.

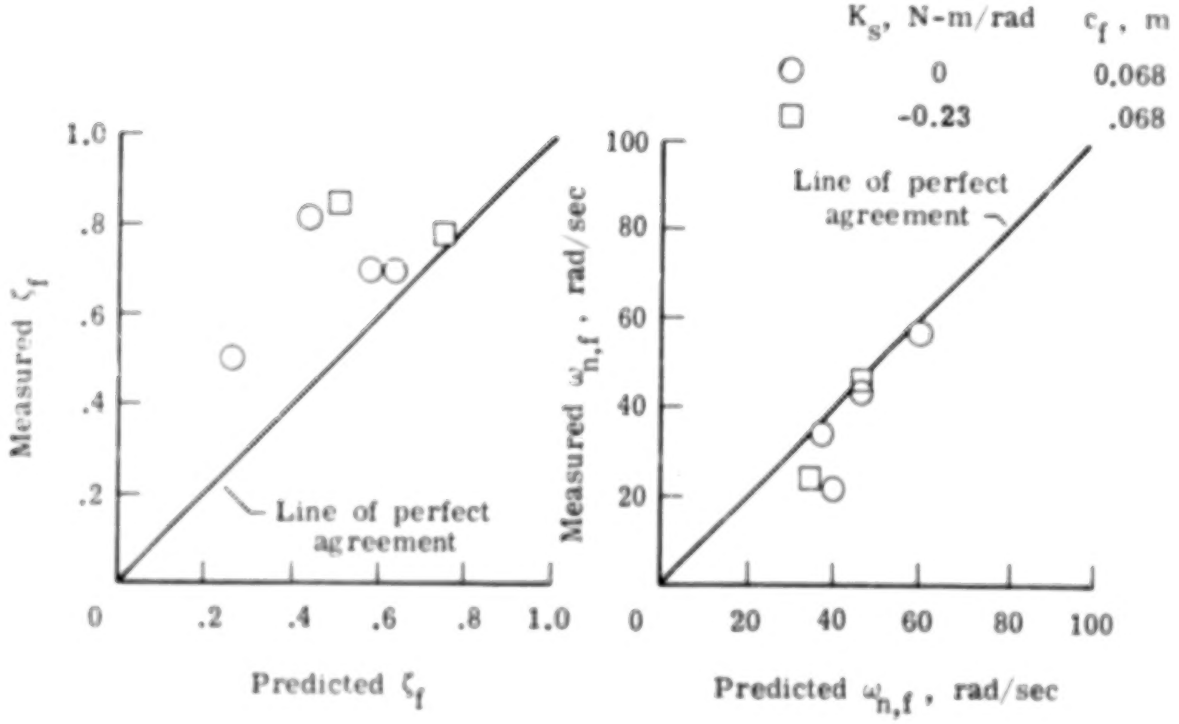

(b) Measured and predicted flap natural frequency and damping.

Figure 10.- Dynamic flap-response characteristics after release from a deflected position with model restrained in heave and pitch.

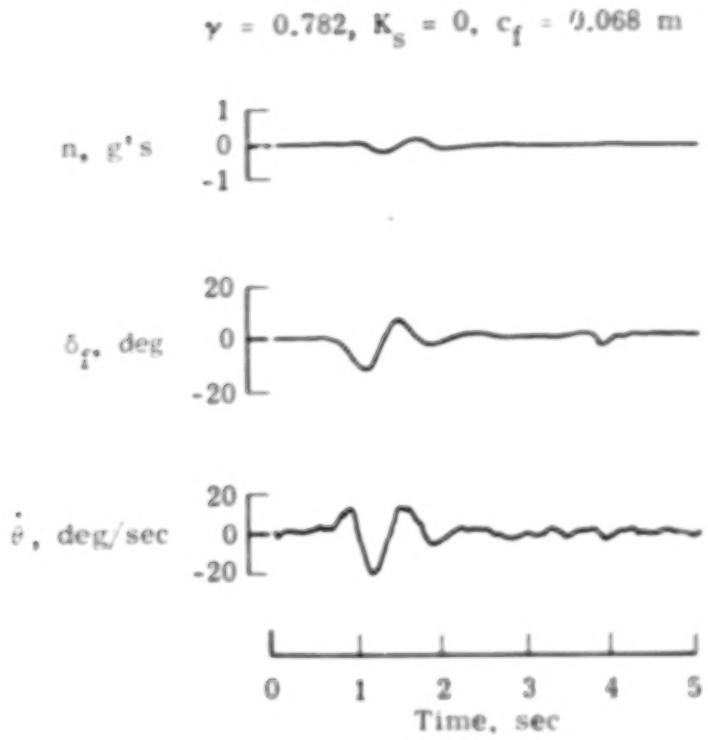

(a) Typical time histories of short-period oscillation.

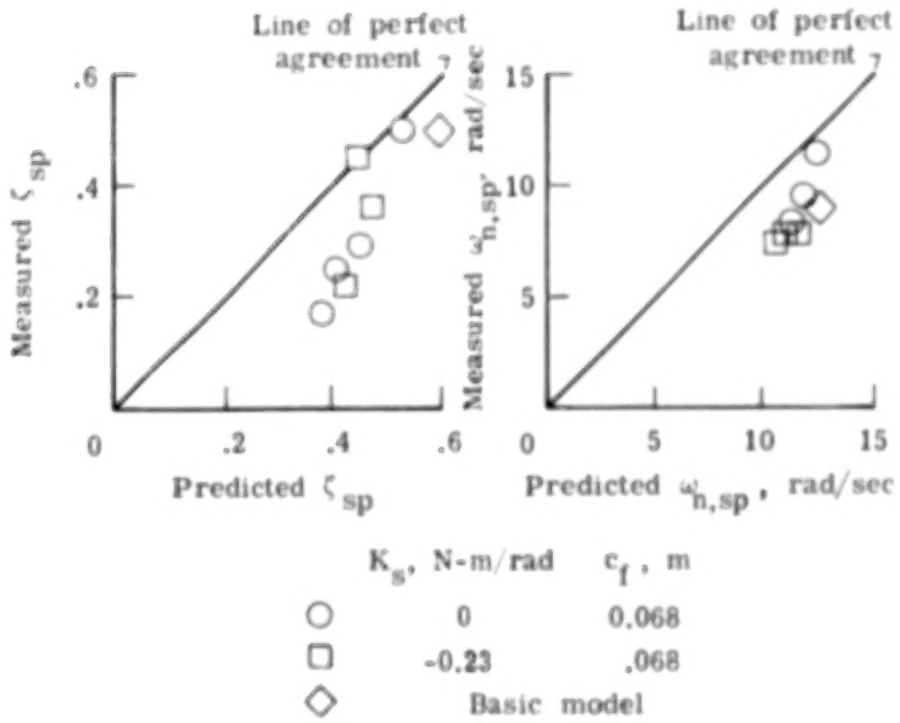

(b) Measured and predicted short-period (sp) natural frequency and damping.

Figure 11.- Model short-period response characteristics.

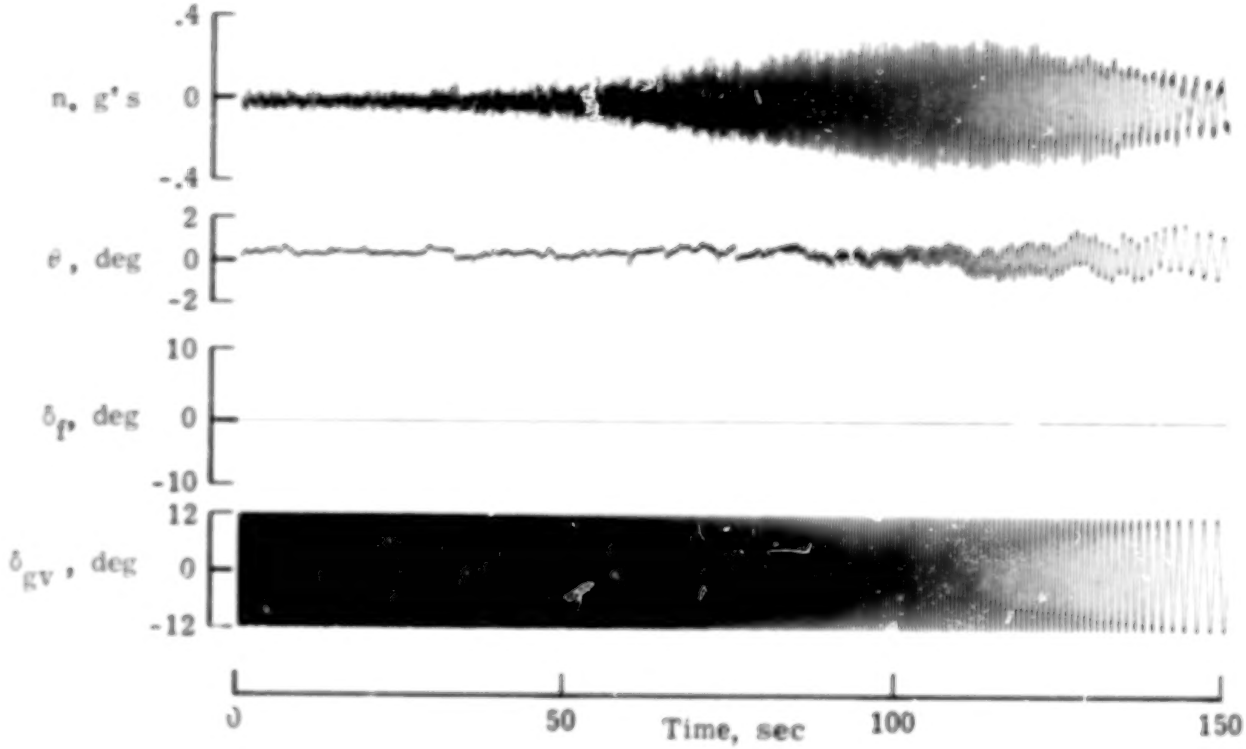

(a) Basic model with flaps fixed (unalleviated).

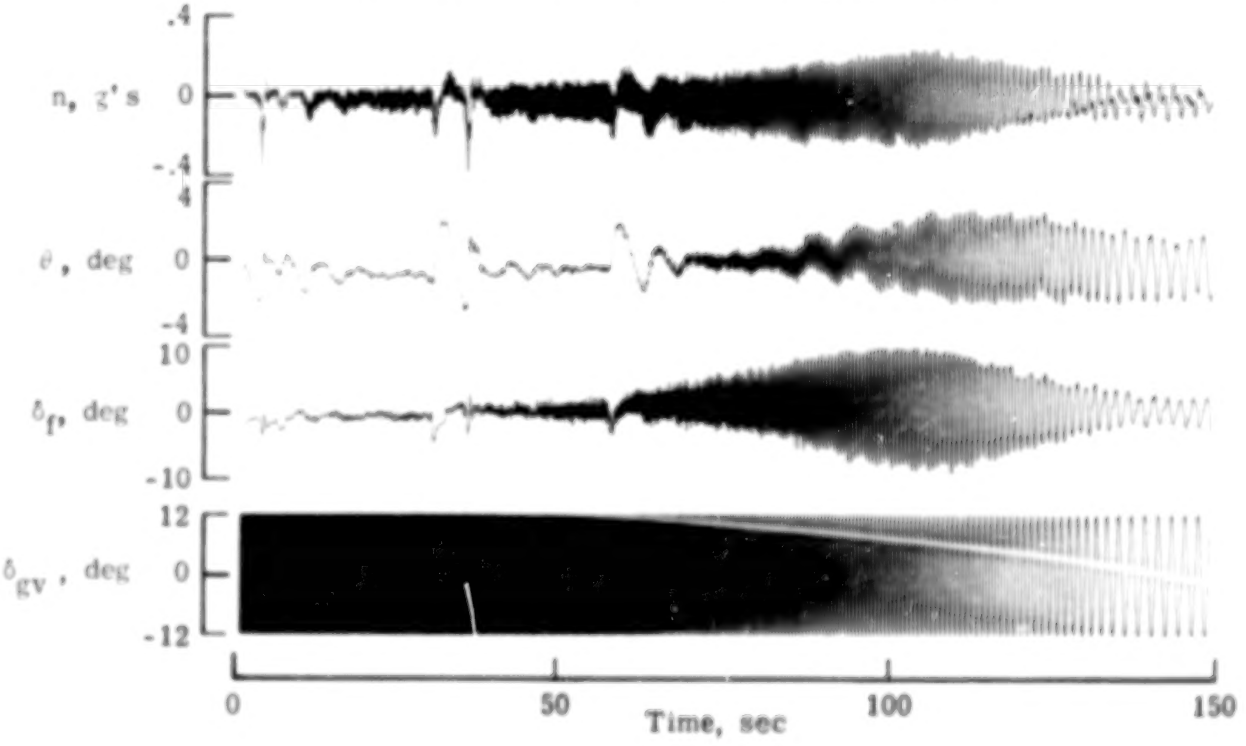

(b) Alleviated model (γ = 0.516, K_g = 0, c_f = 0.068 m).

Figure 12.- Time-history response of model to gusts generated by sweeping TDT gust vanes from about 5 Hz to 0.5 Hz.

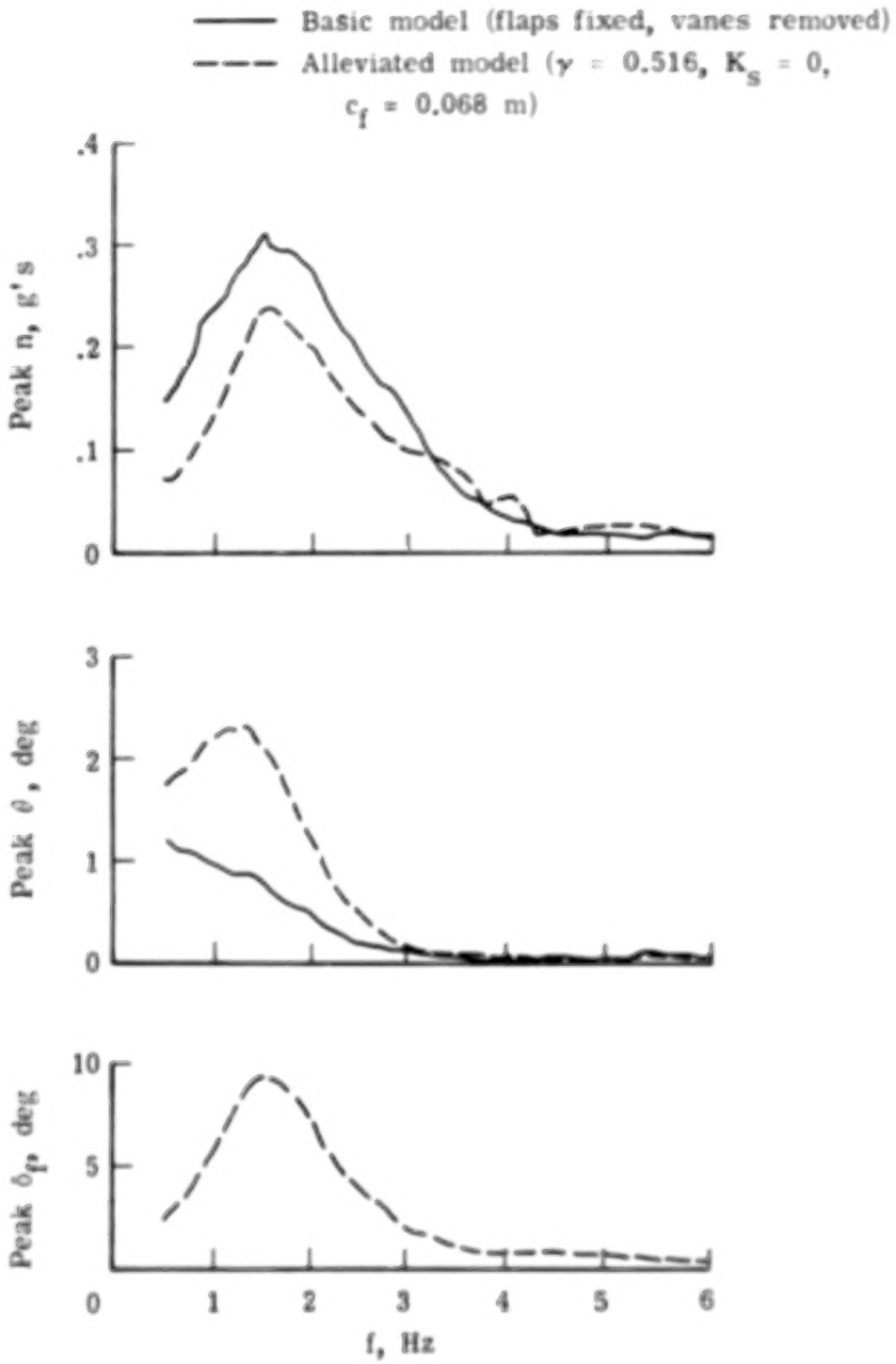

Figure 13.- Peak model responses as a function of frequency.

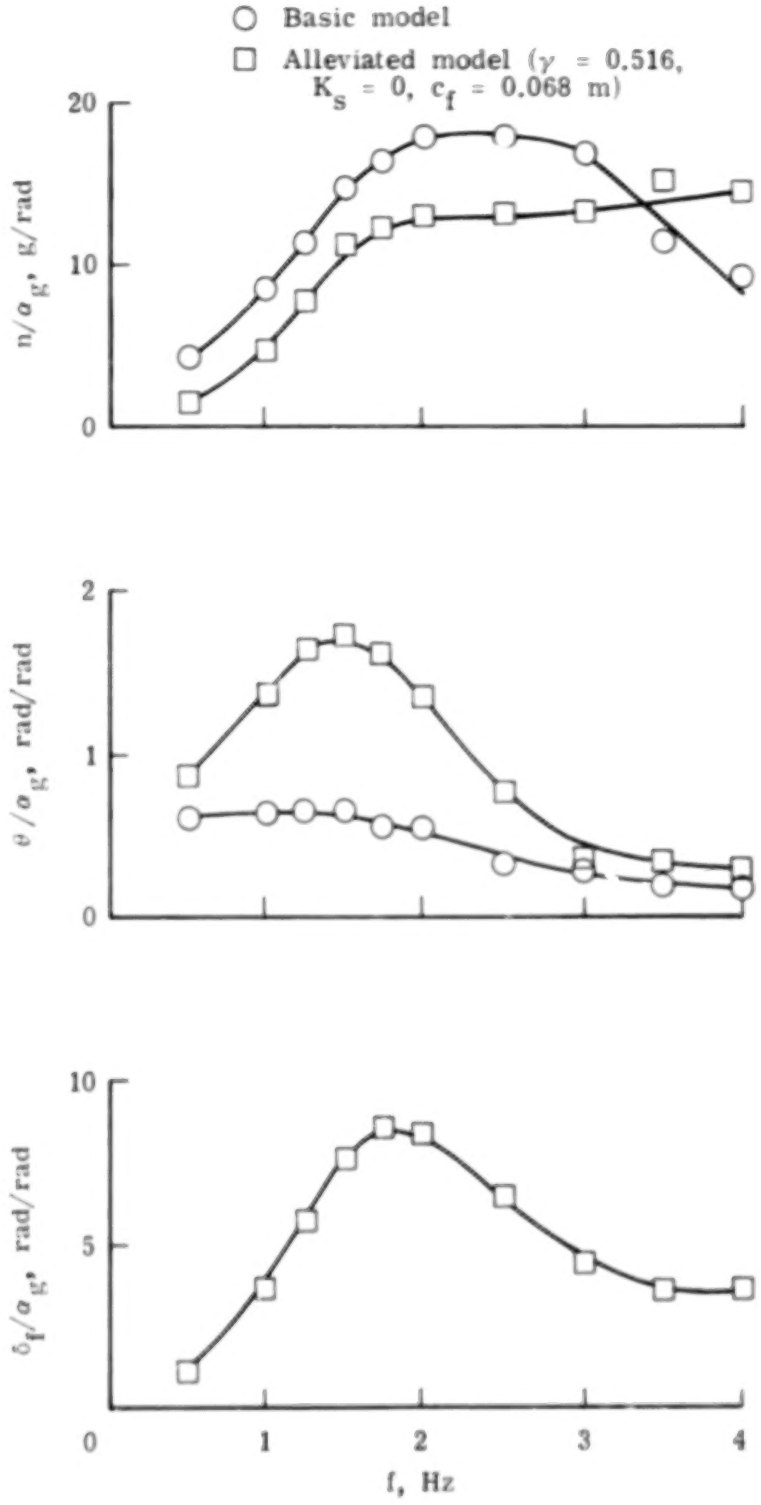

Figure 14.- Model frequency response (model response divided by gust angle).

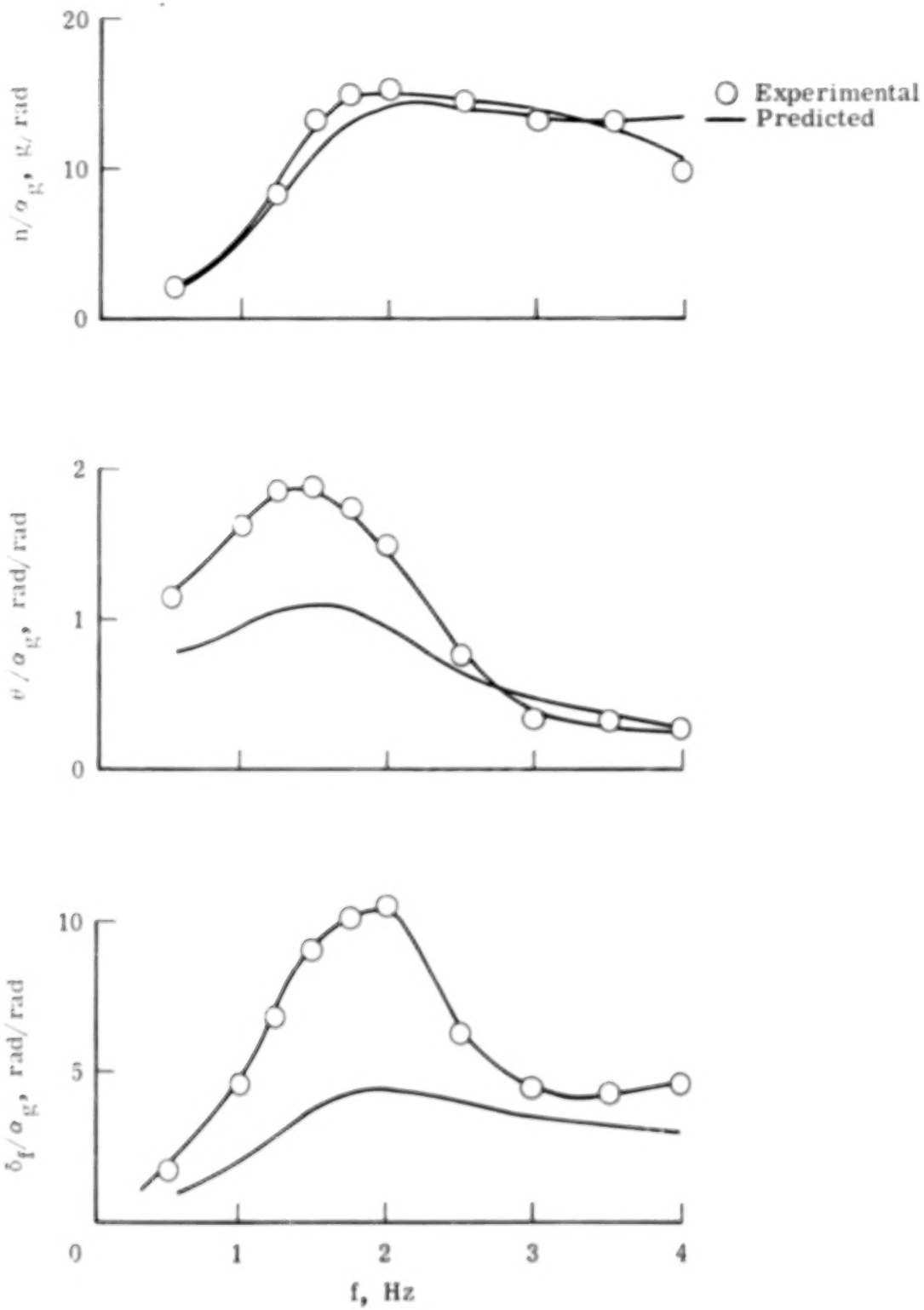

(a) Alleviated model (γ = 0.691, K_s = 0, c_f = 0.068 m).

Figure 15.- A comparison of measured and theoretically predicted model responses.

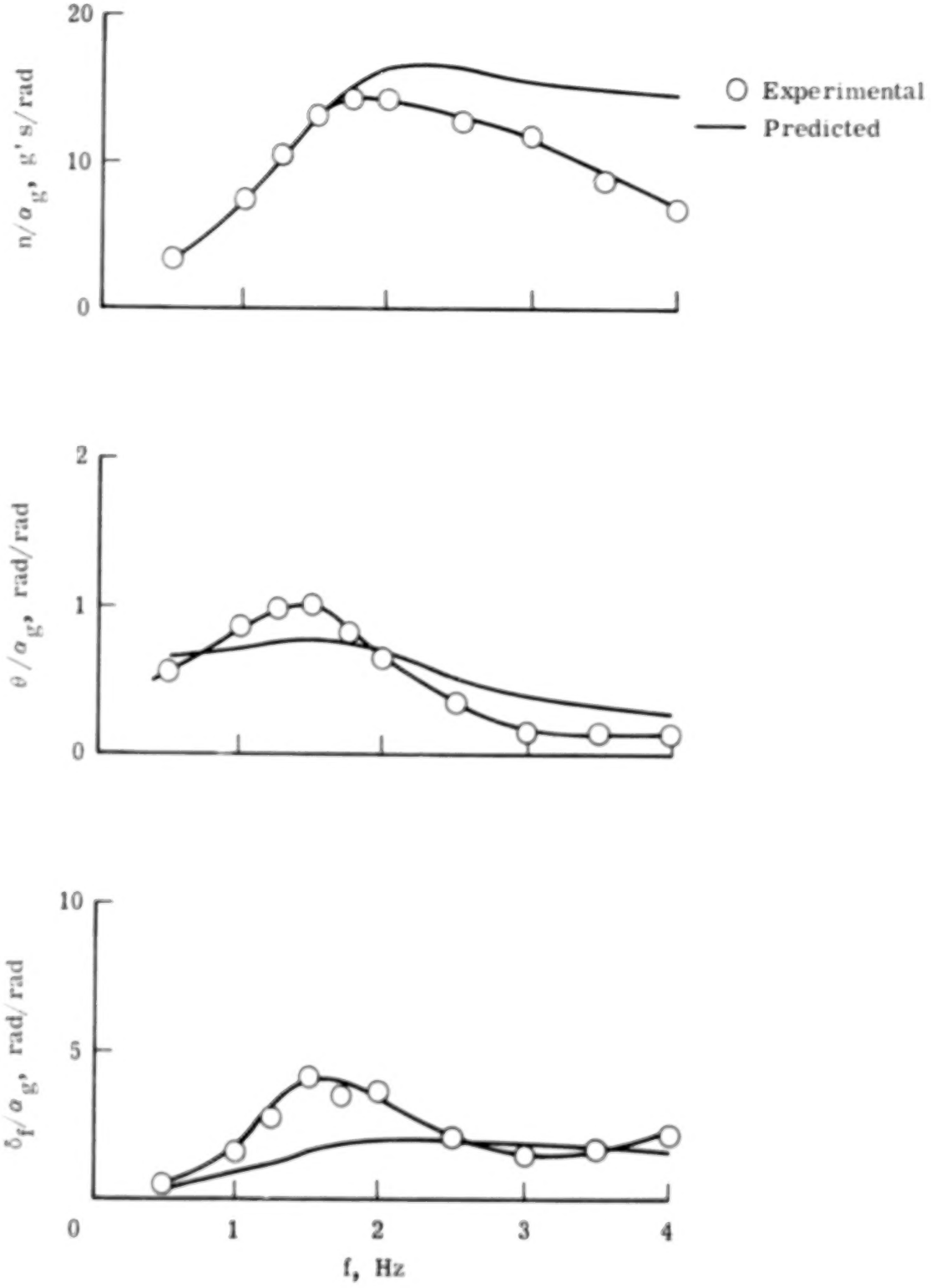

(b) Alleviated model (γ = 0.516, K_s = -0.23 N-m/rad, c_f = 0.068 m).

Figure 15.- Concluded.

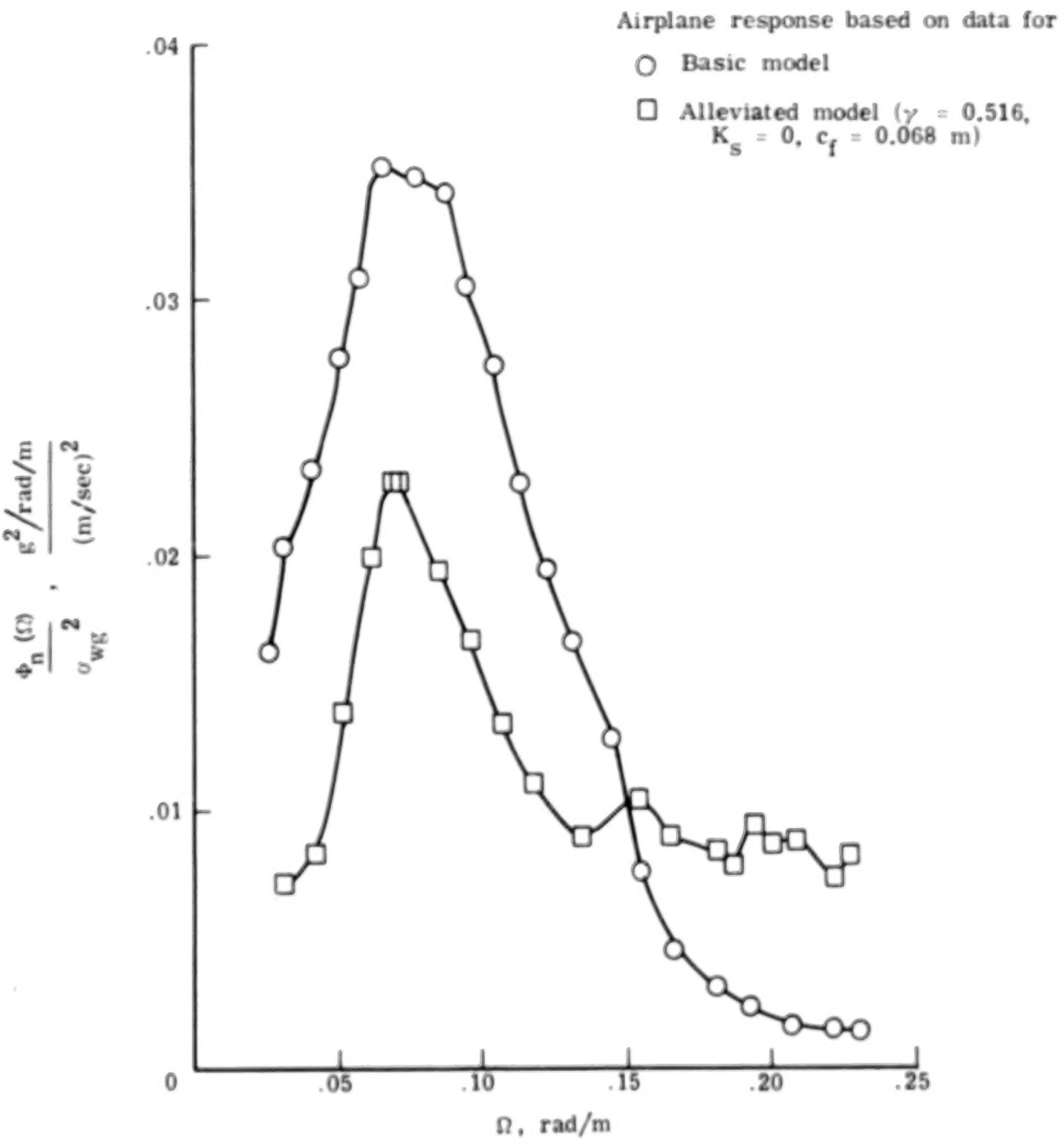

Figure 16.- Power of spectrum of nominal acceleration for a full-scale airplane in atmospheric turbulence based on model-response measurements.

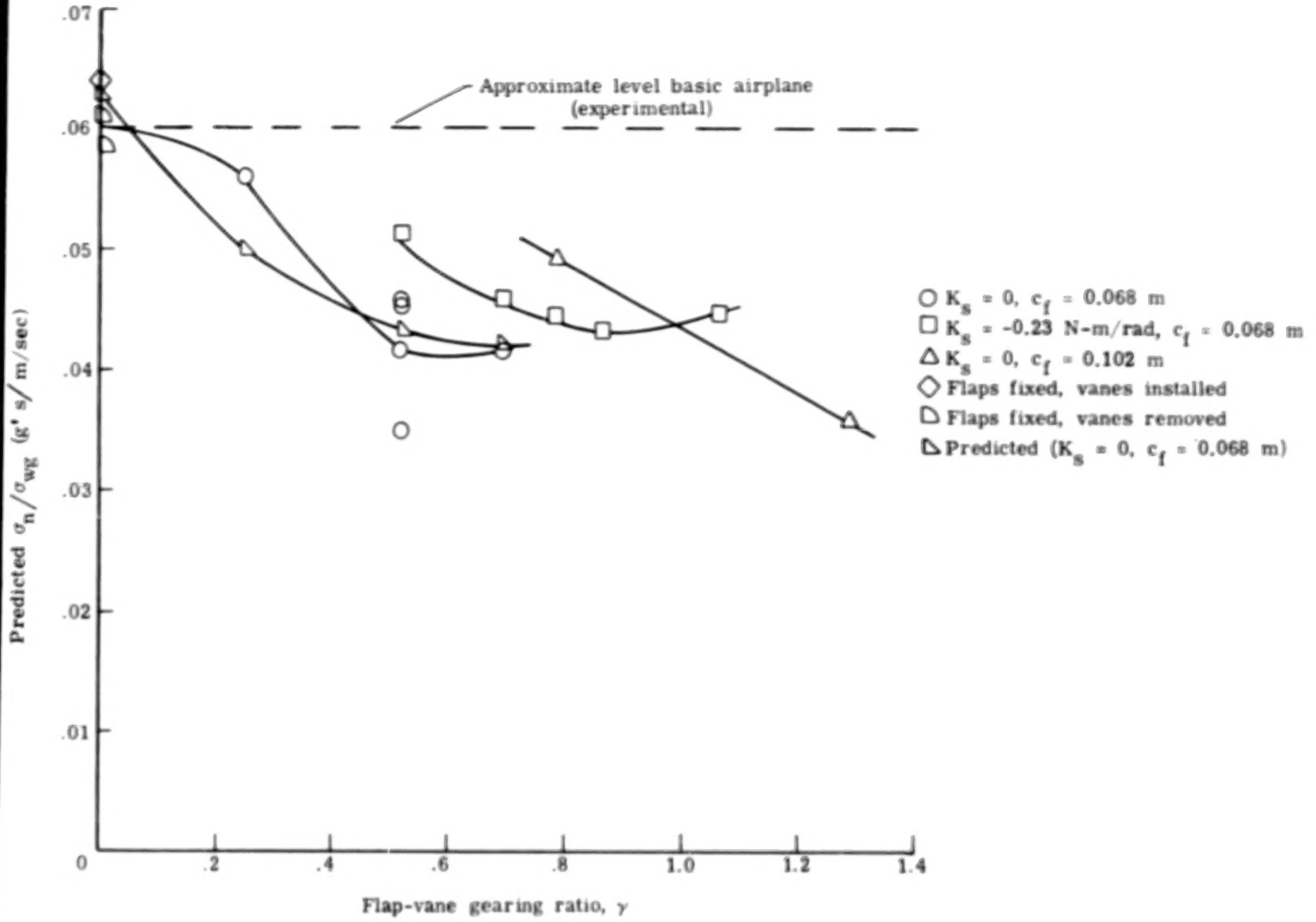

Figure 17.- The rms normal acceleration for a full-scale airplane in atmospheric turbulence based on model-response measurements.

90

50

END

5.19 78